Journal of Molecular Liquids 375 (2023) 121351

Contents lists available at ScienceDirect

Journal of Molecular Liquids

journal homepage: www.elsevier.com/locate/molliq

Facilitated solvent screening for membrane-based extraction of chiral amines via *a priori* simulations

Gilles Van Eygen [a,b,*], Daan Mariën [a], Anja Vananroye [c], Christian Clasen [c], Bart Van der Bruggen [a], Anita Buekenhoudt [d], João A.P. Coutinho [e], Patricia Luis [b,f]

[a] Process Engineering for Sustainable Systems (ProcESS), KU Leuven, Celestijnenlaan, 200f, 3001 Leuven, Belgium
[b] Materials & Process Engineering (IMAP), UC Louvain, Place Sainte Barbe 2, B-1348 Louvain-la-Neuve, Belgium
[c] Soft Matter, Rheology and Technology (SMaRT), KU Leuven, Celestijnenlaan, 200f, 3001 Leuven, Belgium
[d] Unit Separation and Conversion Technology, Vlaamse Instelling voor Technologisch Onderzoek, VITO NV, Boeretang 200, 2400 Mol, Belgium
[e] CICECO-Aveiro Institute of Materials, Chemistry Department, University of Aveiro, 3810-193 Aveiro, Portugal
[f] Research & Innovation Centre for Process Engineering, ReCIPE, Place Sainte Barbe 2, bte L5.02.02, B-1348 Louvain-la-Neuve, Belgium

ARTICLE INFO

Article history:
Received 25 October 2022
Revised 9 January 2023
Accepted 27 January 2023
Available online 31 January 2023

Keywords:
Ionic liquids
Supported liquid membranes
Extraction technology
COSMO-RS

ABSTRACT

Chiral amines are important building blocks in the pharmaceutical industry. A challenge for the current industry is their difficult synthesis procedures, which employ harsh operating conditions or have an unfavourable equilibrium constant. An interesting strategy in improving the reaction equilibrium is the use of *in-situ* product removal via membrane extraction (ME) using supported liquid membranes (SLM), which is explored in this work. More specifically, the separation of the product amines α-methylbenzylamine (MBA) and 1-methyl-3-phenylpropylamine (MPPA) from the donor amine isopropyl amine (IPA) by employing SLMs is investigated in this study. A difficulty in SLM-applications is the solvent selection, which mostly requires the use of extensive liquid–liquid extraction (LLE) testing. In this work, COSMO-RS is used to perform a fast and simplified screening of almost 400 ILs, which led to a shortlist definition of fourteen ILs. For these fourteen ILs, critical solvent properties (i.e., density, viscosity and phase miscibility) were analysed experimentally and compared to simulations in COSMO-RS. Finally, four promising ionic liquids were selected for further LLE- and ME-testing, namely trihexyltetradecylphosphonium bis (trifluoromethylsulfonyl)imide ([P6,6,6,14][N(Tf)2]), 1-methyl-1-propylpyrro-lidinium bis(trifluorome thylsulfonyl)imide ([C3mPyr][N(Tf)2]), 1-hexyl-3-methylimidazolium bis(trifluoromethylsulfonyl)imide ([C6mim][N(Tf)2]) and triethylsulfonium bis(trifluoromethylsulfonyl)imide ([S2,2,2][N(Tf)2]). Based on wettability testing of four polymeric porous substrates (i.e., PTFE, PES, PSf and PVDF), the PTFE-support was chosen for the stability tests, due to its very high hydrophobicity. The LLE- and stability tests showed that [P6,6,6,14][N(Tf)2] has the highest MBA/IPA- and MPPA/IPA-selectivity and the best SLM-stability of all the tested ILs. Comparative SLM-testing with the benchmarking solvent undecane showed that the IL [P6,6,6,14][N(Tf)2] has a higher SLM-selectivity than undecane at elevated temperatures, while no decrease in its stability was observed.

1. Introduction

Chiral amines are key intermediates for a myriad of bioactive compounds, used in the chemical, agrochemical and pharmaceutical industries. It is estimated that chiral amines are present in 40 to 45 % of drug candidates [1,2]. Examples of pharmacologically important chiral amines are α-methylbenzylamine (MBA), which is used as a chiral ligand, auxiliary and base and in the development of new organo-catalysts; and (*R*)-(+)-1-methyl-3-phenylpropylamine (MPPA), which is a precursor of the anti-hypertensive dilevalol [3,4]. These compounds can be produced by both chemical and biocatalytic synthesis. However, finding effective synthesis routes is still a major challenge [5].

The chemical synthesis of chiral amines is typically performed under high temperature and pressure and using a precious and toxic heavy metal catalyst (i.e., nickel or cobalt supported on silica or alumina). Generally, these reactions have insufficient stereoselectivity and suffer from a catalyst-contaminated product stream, which necessitates additional purification steps. On the other hand, biochemical synthesis of these amines using enzymes shows excellent chemo-, regio- and enantioselectivity, and simplifies the

* Corresponding author.
E-mail address: gilles.vaneygen@kuleuven.be (G. Van Eygen).

https://doi.org/10.1016/j.molliq.2023.121351
0167-7322/

overall process. Several classes of enzymes have already been identified for chiral amine synthesis, such as amine dehydrogenases, monoamine oxidases, imine reductases and reductive aminases. Especially, the use of ω-transaminases (TAs) as enzymatic catalysts has been proven effective for chiral amine synthesis. TAs are enzymes that catalyse the transfer of an amine group to a prochiral acceptor ketone, resulting in a chiral amine and a coproduct ketone. Isopropyl amine (IPA) is mostly used as the donor amine, as it is an economical achiral amine. In addition, the removal of the reaction by-product acetone is easily done via evaporation [6–9].

Chiral amines can be synthesised using TAs via two routes [10–12], namely kinetic resolution of a racemic amine mixture and direct asymmetric synthesis from prochiral ketones, which are both shown in Fig. 1. The former strategy is commonly used in industry nowadays, despite its maximum theoretical yield of 50 %. Its yield can be improved, however, if a racemisation step is included. The asymmetric synthesis procedure, on the other hand, has a theoretical yield of 100 %. It should be noted that this high yield is only achieved by shifting the equilibrium to the product side, as the equilibrium is strongly in favour of the amine donor.

Different strategies have already been proposed to overcome the thermodynamic limitations in chiral amine syntheses, namely addition of an excess of the amine donor [6], auto-degradation of the coproduct [13], use of enzymatic cascades [14,15], whole-cell catalysis [16,17] and *in-situ* product removal (ISPR). Especially *in-situ* product removal, which removes the product amine from the reaction medium, has been shown to effectively shift the equilibrium to enhance the yields. Liquid-liquid extraction (LLE), adsorption, evaporation and distillation are all possible methods for *in-situ* product removal of the product amine [10,11]. An interesting strategy for *in-situ* product removal is membrane extraction (ME) using supported liquid membranes (SLM). An SLM usually consists of a porous support material in which an extractant phase is immobilised, as can be seen schematically in Fig. 2. The target compound in the feed solution are extracted into the liquid membrane (LM) phase and simultaneously stripped into the strip solution. SLMs have different advantages over conventional LLE, such as the need for only small amounts of the extractant and the combination of extraction and stripping in one module [18]. Rehn et al. [19,20] already investigated the use of a polypropylene, hollow fibre SLM-contactor for the separation of α-methylbenzylamine (MBA) and 1-methyl-3-phenylpropylamine (MPPA) from isopropyl amine (IPA) with undecane as the selective extractant. Their setup showed a high selectivity towards MBA and MPPA and a stability of more than 30 h. However, this stability might be too low for industrial applications. To this end, the use of other extractants should be investigated.

The selection of appropriate extractants for specific applications is an inherent difficulty in SLM-separations. Different requirements of the extractant have been suggested. The most important requirement is a high solubility towards the target compound in the feed mixture, leading to a high selectivity and efficiency. Furthermore, the extractant should have a suitable viscosity to allow for simple impregnation and be non-volatile [21]. A myriad of different carriers and extractants has been used in the literature, making the selection of suitable extractants cumbersome. Especially, ionic liquids (ILs) are deemed to be excellent extractants, due to their tunable solubility behaviour, low vapor pressure and high thermal stability. ILs are salts consisting of organic cations and (in)organic anions. It is suggested that by combination of different cations and anions and by mixing different ILs, up to 10^{18} ILs can be prepared [22,23]. This challenges the current selection procedure, which is mostly based on comparative LLE-experiments.

A possibility is to model the solubility behaviour using *ab initio* modelling tools, such as COSMO-RS, although this approach has not yet been used extensively for ME-applications. COSMO-RS is an *a priori* predictive model for thermodynamic equilibrium calculations of fluids. More specifically, COSMO-RS allows to predict chemical potentials from surface charges of a certain molecule within a conductor, via quantum-chemical calculations [24,25]. COSMO-RS has already been used for ionic liquid screening for a variety of applications, amongst others, fractionation of terpenes and terpenoids [26,27], separation of benzene and cyclohexane [28], lithium extraction [29], gas separations [30], recovery of lactic acid [31], azeotropic separations [32] and naphthenic acid extraction [33]. Furthermore, Gou et al. [25] and Janoschek et al. [34] have used COSMO-RS for the screening of conventional organic extractants for SLM-applications.

In the present study, different RTILs were characterised to enable a rationalised extractant selection for the separation of chiral amines. First, COSMO-RS was used to determine critical solvent properties (i.e., density, viscosity, phase miscibility and selectivity) of a variety of room temperature ionic liquids (RTILs) *ab initio*, after which these properties were validated experimentally. More

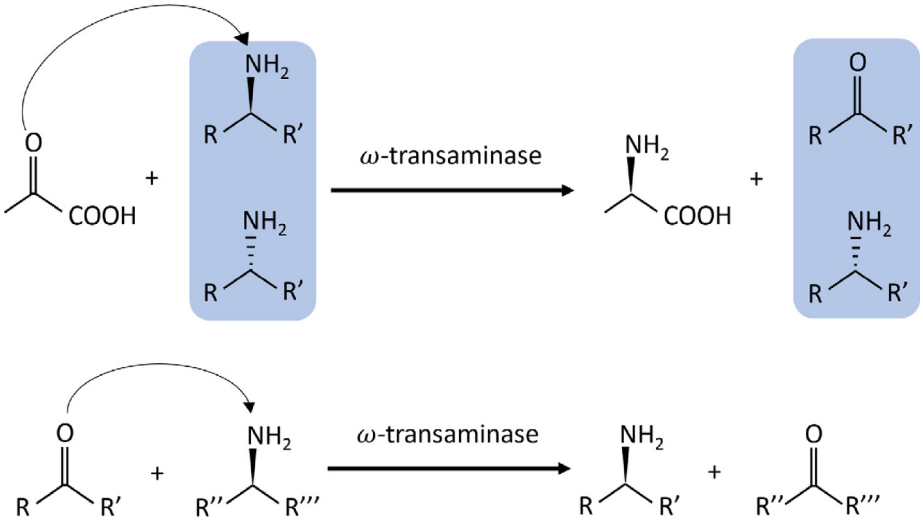

Fig. 1. Preparation of chiral amines by kinetic resolution of a racemic amine mixture (top) or asymmetric synthesis of prochiral ketones (bottom), based on Koszelewski et al. [10].

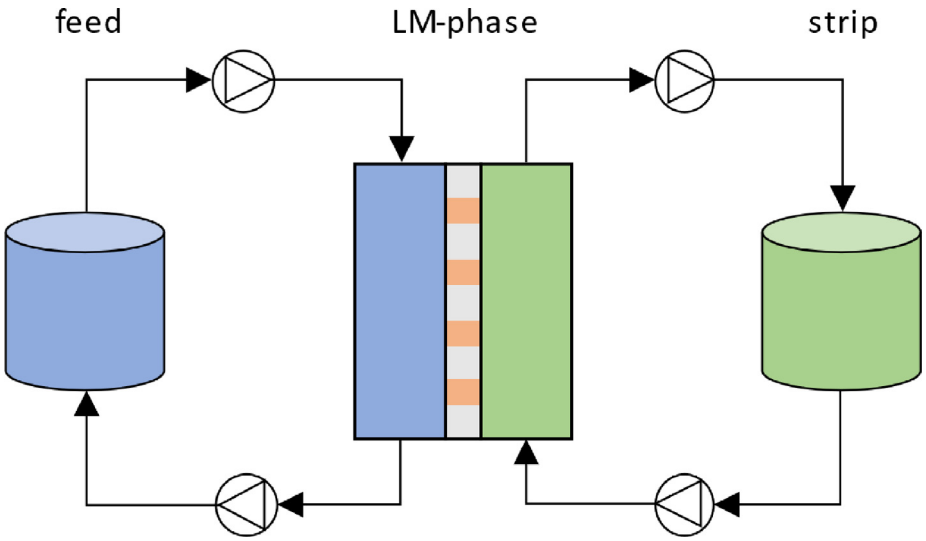

Fig. 2. Schematic drawing of a membrane extraction setup, using a supported liquid membrane setup, based on Van Eygen et al. [18]. The LM-phase (orange) is immobilised in the pores of the support material. (For interpretation of the references to colour in this figure legend, the reader is referred to the web version of this article.)

specifically, fourteen RTILs were considered as candidates for SLM-extraction of chiral amines, i.e., selectively separating the product amines MBA and MPPA from the donor amine IPA. Second, the wettability of the ILs on four different commercial membranes was tested to select the most suitable support material. Third, the extraction efficiency and stability of four promising RTILs were tested in conventional LLE- and SLM-tests and linked to critical solvent properties. Finally, the effect of temperature on the extraction performance of the optimal IL was investigated.

2. Materials and methods

2.1. Chemicals and membranes

The following chemicals were used for the extraction experiments. Na_2CO_3 (≥99.5 %, Honeywell Fluka, Germany) and $NaHCO_3$ (≥99.7 %, Sigma-Aldrich, Germany) were used to prepare the feed buffer. NaH_2PO_4 (≥99.0 %, Sigma-Aldrich, Germany) and H_3PO_4 (≥85 %, Sigma-Aldrich, Switzerland) were used to prepare the strip buffer. NaOH (≥98 %, Sigma-Aldrich, Germany) and HCl (37 %, Acros Organics) were used to prepare an alkaline solution for pH-adjustment. The used amines were isopropyl amine (≥99.5 %, Sigma-Aldrich, Belgium), 1-methyl-3-phenylpropylamine (98 %, Sigma-Aldrich, Germany) and α-methylbenzylamine (98 %, Sigma-Aldrich, Germany). The internal standard used for the GC-analysis was triethylamine (99 %, Acros Organics). Undecane (99 %, Acros Organics, China) was used as a conventional organic extractant, whilst Aliquat-336 (TG, Alfa Aesar) was used as a benchmarking ionic liquid. The fourteen studied ionic liquids, which were all purchased from Iolitec, are given in Table 1. All chemicals were used without further purification. The molecular structures of the cations and anions are given in the Supplementary Information SD-1 and SD-2, respectively. The support materials used in this study are given in Table 2.

2.2. Experimental analysis of critical solvent parameters

The density and viscosity of the ionic liquids were determined with a Lovis 2000 ME rolling-ball type viscometer (Anton Paar). Three different-sized capillaries were used with a diameter of 1.59, 1.8 and 2.5 mm. The samples were measured at 25 °C, with a maximum variation coefficient set at 1 % and an angle of 70°.

Table 1
Cation and anion name and purity of the considered ionic liquids.

Cation	Anion	Purity [%]
1-Butyl-3-methylimidazolium	Hexafluorophosphate	99
1-Butyl-3-methylimidazolium	Tricyanomethanide	> 98
1-Butyl-3-methylimidazolium	Bis(trifluoromethylsulfonyl) imide	99
1-Butyl-3-methylimidazolium	Bis(perfluoroethylsulfonyl) imide	99
Trihexyltetradecylphosphonium	Bis(trifluoromethylsulfonyl) imide	> 98
1-Methyl-1-propylpyrrolidinium	Bis(trifluoromethylsulfonyl) imide	99
1-Hexyl-3-methylimidazolium	Bis(trifluoromethylsulfonyl) imide	98
1-Butyl-3-methylpyridinium	Bis(trifluoromethylsulfonyl) imide	99
1-Allyl-3-methylimidazolium	Bis(trifluoromethylsulfonyl) imide	> 99
1-Benzyl-3-methylimidazolium	Bis(trifluoromethylsulfonyl) imide	> 99
1-Propyl-3-methylpyridinium	Bis(trifluoromethylsulfonyl) imide	99
1-(2-Methoxyethyl)-3-methylimidazolium	Bis(trifluoromethylsulfonyl) imide	> 98
Triethylsulfonium	Bis(trifluoromethylsulfonyl) imide	99
1-Butyl-3-vinylimidazolium	Bis(trifluoromethylsulfonyl) imide	98

Table 2
Considered support materials, with indication of their pore size and supplier.

Material	Pore size [nm]	Support	Supplier
Polysulfone (PSf)	100	PP	Alfa-Laval
Polyvinylidene difluoride (PVDF)	100	PP	Synder Filtration
Polyethersulfone (PES)	90	PP	Synder Filtration
Polytetrafluoroethylene (PTFE)	100	PP	Donaldson
Polytetrafluoroethylene (PTFE)	50	/	Donaldson

Additionally, the sample density was measured. Between different samples the equipment was cleaned with acetone and water. Each reported value was an average of triplicate measurements.

To determine the phase miscibility of the ionic liquids with aqueous phases, the following experiments were performed. The IL was added to a centrifuge tube with Milli-Q water in a 1:2 volumetric ratio. The test tubes were closed off with a cap and placed in a lab shaker for 24 h at 120 rpm and 30 °C. After shaking, the samples were taken out of the shaker and were left unattended for 24 h to let the phases settle. After settling, a sample of the water-saturated IL-phase was taken and analysed with the V30S Volumetric Karl Fischer Titrator (Mettler Toledo) in combination with a Stromboli oven (Mettler Toledo). The Stromboli oven was used at a temperature of 150 °C to evaporate the water from the IL-phase. Additionally, a sample was taken from the IL-saturated aqueous phase and was pipetted on a petri dish. The petri dish was placed on a heating plate at 105 °C for 15 min, after which the weight was recorded. The IL-content in the aqueous phase x_{IL} was then determined using the following equation:

$$x_{IL}(wt\%) = \frac{m_{residual}}{m_{sample}} \tag{1}$$

where m_{sample} and m_{res} are the sample mass (g) and the residual sample mass after evaporation (g), respectively. The experiments were performed at least in duplicate.

To measure the contact angle of the considered ILs on various substrates, a Biolin Scientific Attension Theta Lite apparatus was used. A 1 mL threaded plunger syringe from Hamilton was used in combination with a disposable needle of stainless steel from Nordson EFD (D_{in} = 0.61 mm, D_{out} = 0.91 ∼ mm, L = 12.7 mm). One drop of the IL was put on the membrane sample, which was fixed to the device platform with double sided tape. All the tested membranes had a polypropylene (PP) support. The drop profile was analysed with the OneAttension software. A typical wetting profile is given in SD-3 in the Supplementary Information. Each measurement was performed in triplicate. Between different samples, the equipment was cleaned with ethanol and water.

2.3. Liquid-liquid extraction experiments

The batch extraction tests were performed in a 1:1 volumetric feed-to-solvent ratio. A test tube was filled with 3 mL of the feed solution and 3 mL of the IL. The feed solution was prepared by adding 3.79 ∼ g of Na_2CO_3 and 5.38 g of $NaHCO_3$ to 500 mL of Milli-Q water. The feed pH was then adjusted to 10 by adding a 25 % HCl- or NaOH-solution. Afterwards, the amines MBA, MPPA and IPA were added to the solution at a concentration of 1000 mg/L. The test tubes were placed in a lab shaker for 24 h at 120 rpm and 30 °C. After shaking, the samples were taken out of the shaker and were left unattended for 24 h to let the phases settle. Afterwards, samples of 1 mL were taken from the aqueous phase for HPLC- and GC-analysis. 15 μL of an internal standard solution of 11.7 g/L triethylamine was added to the GC-samples. The extraction performance was determined using the extraction efficiency E, which is defined as follows:

$$E = \frac{C_{org}V_{org}}{C_{org}V_{org} + C_{aq}V_{aq}} = \frac{C_{org}V_{org}}{C_{feed}V_{feed}} \tag{2}$$

in which C_{org}, C_{aq} and C_{feed} are the concentrations of the solute in the organic and aqueous phase after the extraction and the initial feed concentration, respectively. V_{org}, V_{aq} and V_{feed} are the volumes of the organic and aqueous phase after the extraction, and the initial volume of the aqueous feed, respectively. Assuming no volume change of the phases occurs, this equation can be adapted to:

$$E = \frac{C_{feed} - C_{aq}}{C_{feed}} \tag{3}$$

To quantify the capability of the extractant to extract more of the target solute compared to the unwanted compound, the selectivity S was defined as follows:

$$S_{MBA/IPA} = \frac{E_{MBA}}{E_{IPA}} \tag{4}$$

$$S_{MPPA/IPA} = \frac{E_{MPPA}}{E_{IPA}} \tag{5}$$

in which E_{MBA}, E_{MPPA} and E_{IPA} are the extraction efficiency of MBA, MPPA and IPA, respectively. The LLE-tests were all performed in triplicate.

2.4. Membrane extraction experiments

Two buffer solutions were prepared for the extraction experiments, namely a feed and a strip buffer at a pH of 10 and 3, respectively. The feed buffer was prepared by adding 1.90 g of Na_2CO_3 and 2.69 g of $NaHCO_3$ to 250 mL of Milli-Q water. After full dissolution, the pH was adjusted to 10 with a 25 % NaOH- or 25 % HCl-solution, after which the amines MBA, MPPA and IPA were added to a final concentration of 500 mg/L. The strip buffer was prepared in a similar manner by adding 5.25 g of NaH_2PO_4 and 431 μL of an 85 % w/w H_3PO_4-solution. After full dissolution, a 25 % NaOH- or 25 % HCl-solution was used to adjust the pH of both the feed and strip to 10 and 3, respectively. All ME-experiments were performed at least in duplicate.

The membrane extraction setup is shown schematically in Fig. 3. The buffer solutions at a volume of 250 mL each were circulated counter-currently using two magnetically driven external gear pumps (Flowtec). The temperature of the buffers was measured using a DIGI-SENSE Data Logging RTD meter. The flow rates and pressures were checked using two variable-area flow meters with valve (100–1000 mL/min, Masterflex) and four Series 3D diaphragm gauge guards with manometer (0–6 bar, EM-Technik), respectively. The temperature of both solutions was kept at the desired temperature by employing a Kiss K6 thermobath (Huber). The membrane cell consisted of two PTFE-parts with a spiral pattern to maximise the contact area. The spiral pattern is also shown in Fig. 3.

The impregnation procedure of the membrane was performed as follows. First, the dry membrane was weighed on a balance. Next, the membrane was soaked overnight or impregnated using vacuum, if undecane or an IL was used, respectively. For the vacuum impregnation, the membrane was placed on a Büchner filtration setup connected to an Edwards high vacuum pump (1 Torr). The IL was pipetted on the membrane surface, until it was fully covered, after which vacuum was applied for at least 30 min. Afterwards, the membrane was weighed again and used for the extraction experiments. After the extraction test, the membrane was patted dry and weighed again to calculate the loss of extractant during the experiment.

During the membrane extraction test, samples of both the feed and strip buffer were taken at the start of the experiment and after 1, 3, 6 and 24 h. At each time point, a 1 mL HPLC- and 1 mL GC-sample was taken. The pH of the strip GC-samples was adjusted by adding 42 μL of a 25 % NaOH-solution. Furthermore, 15 μL of an internal standard solution of 11.7 g/L TEA was added to the GC-samples of both the feed and strip. The MBA- and MPPA-concentrations were determined via an HPLC-UVVIS (Schimadzu Prominence-I LC-2030C 3D) using gradient elution with acetonitrile and 0.1 v% H_3PO_4 as the mobile phases. The IPA-concentration was determined via a headspace GC-FID Autosystem XL (PerkinElmer) with helium as the mobile phase. The GC used an Rtx-5 Amine column (30 m, 0.25 mm, 0.50 μm).

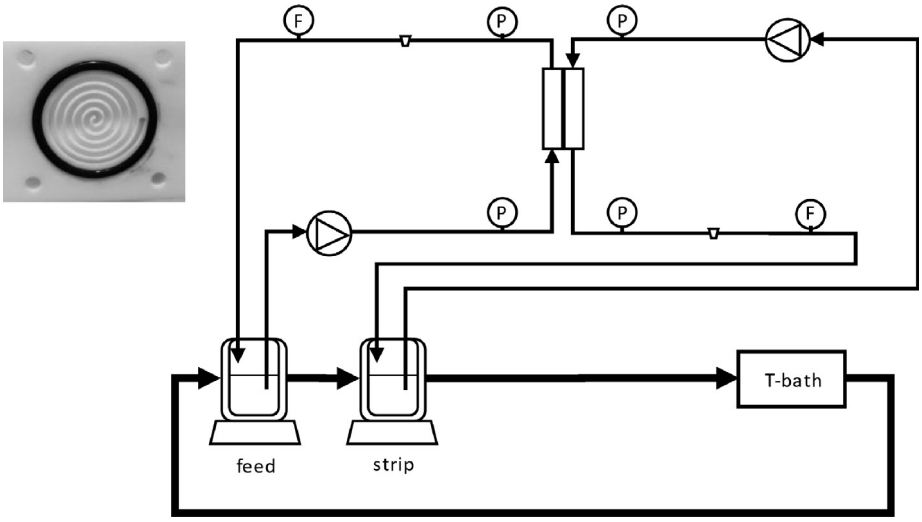

Fig. 3. Schematic drawing of the used membrane extraction setup and indication of the spiral pattern (top left).

2.5. COSMO-RS simulations

First, the TmoleX v. 4.5 software package was used to perform the quantum calculations using the density functional theory (DFT) with a resolution identity (RI) approximation. Vibrational frequency calculations allowed for the determination of an electronic energy minimum. The optimized geometries of the considered cations and anions were obtained using a triple zeta valence polarised basis set (def-TZVP), the Becke-Perdew (BP-86) functional level of theory and the COSMO solvation model, and were stored as COSMO-files. Second, the vibrational frequency calculations were executed to confirm the presence of an optimized energy state. Third, the generated COSMO-files were used as input in COSMOthermX to predict the thermodynamic properties of the considered ionic liquids. The ionic liquids were simulated by using a molecular model of independent counterions, i.e., an equimolar cation–anion mixture [31,32,35].

3. Results and discussion

3.1. COSMO-RS simulations

3.1.1. Anion and cation selection

First, COSMO-RS was used to screen and make a shortlist of suitable ionic liquid candidates for the separation of MBA and MPPA from IPA. As mentioned before, the solubility towards the target solutes is one of the main solvent criteria, in addition to the selectivity. The affinity between the solvent and the solute can be predicted using activity coefficients at infinite dilution γ^{∞} [24]. More specifically, the difference in γ^{∞} for a pair of solutes is related to the IL-selectivity for the separation case at hand. The activity coefficient of a certain solute is obtained from the following formula [36]:

$$\gamma = \exp\left(\frac{\mu - \mu^0}{RT}\right) \tag{6}$$

in which μ and μ^0 are the chemical potential of the solute in a mixture and the pure state, R is the universal gas constant and T is the temperature. The activity coefficient at infinite dilution is obtained by taking the limit $\gamma^{\infty} = \lim_{x \to 0} \gamma$. In particular, the solute–solvent interaction weakens if $\gamma^{\infty} > 1$, which is due to the positive deviation of Raoult's law. On the other hand, the affinity becomes stronger for $\gamma^{\infty} < 0.1$, while the solvent shows a moderate solute affinity for $0.1 < \gamma^{\infty} < 1$ [37].

The γ^{∞}-values can then be used to determine the IL-selectivity, for which the definition in Equation (7) is mostly used [26–29]. However, for applications using supported liquid membranes (SLM), it is necessary to alter this definition to Equation (8) in which the SLM-selectivity is defined by the ratio of the partition coefficients $K_j^{1,2}$ and $K_i^{1,2}$ of the by-product j and the target solute i between phases 1 and 2, which denote the aqueous feed and the ionic liquid, respectively. The by-product and target solutes are IPA and MBA or MPPA, respectively.

$$S_{ij}^{\infty} = \frac{\gamma_j^{\infty}}{\gamma_i^{\infty}} \tag{7}$$

$$S_{ij}^{\infty} = \frac{K_j^{1,2}}{K_i^{1,2}} = \frac{\left(\frac{\gamma_{j,2}^{\infty}}{\gamma_{j,1}^{\infty}}\right)}{\left(\frac{\gamma_{i,2}^{\infty}}{\gamma_{i,1}^{\infty}}\right)} \tag{8}$$

The MBA/IPA- and MPPA/IPA-selectivity results are presented in Fig. 4 for a variety of cations and anions. More specifically, thirteen ammonium-based, thirty-one imidazolium-based, thirteen pyridinium-based, two piperidinium-based, five pyrrolidinium-based, three sulfonium-based, eight phosphonium-based and four other cations, i.e., betaine, choline, N,*N*-diethyl-*N*-methyl-N-(2-methoxyethyl)ammonium and 1-hexyl-1,4-diazabicyclo[2.2.2]octa nium, were used for the selectivity simulations. Only five anions were considered in the simulations, as only a limited number of anions can be considered as hydrophobic. Cláudio et al. [38] simulated the hydrogen-bond basicity, which is a measure for their polarity, for [C4mim]-based ILs with various anions. Based on their results, they showed that fluorine-based anions, such as $[PF6]^-$ and $[BF4]^-$, have the highest hydrogen-bond accepting ability. However, the [PF6]-anion may break down into HF in the presence of water. Opposed to these unstable anions, water-stable anions include $[N(Tf)2]^-$, $[FSI]^-$, Cl^- and $[DCA]^-$ [39]. However, Cl^- and $[DCA]^-$ are hydrophilic, according to Cláudio et al. [38]. Therefore, four hydrophobic anions were selected, which can be ranked according to their hydrogen-bonding interaction energy as follows:

$$[C(CN)3]^- < [N(Tf)2]^- < [BETI]^- < [PF6]^-$$

Pereira et al. [40] also showed that for [C4mim]-based ionic liquids, a similar ranking ($[C(CN)3]^- < [N(Tf)2]^- < [PF6]^-$) could be found for the contact angle of these ILs on hydrophilic glass surfaces, which validates their hydrophobicity. Additionally, the [FSI]-anion was selected, as it is similar in structure to the anions $[N(Tf)2]^-$ and $[BETI]^-$.

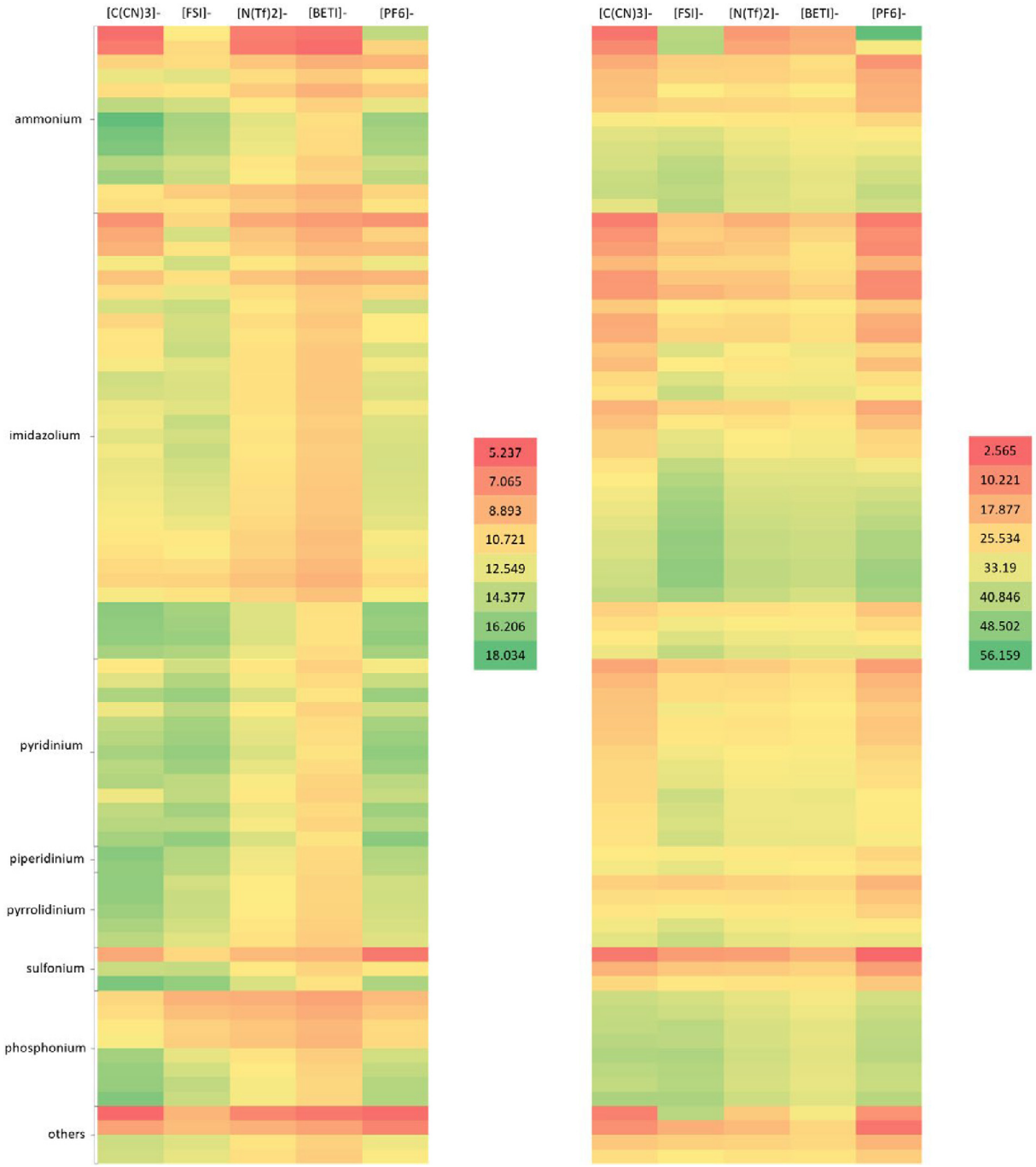

Fig. 4. MBA/IPA- (left) and MPPA/IPA-selectivity (right) for various cations combined with five hydrophobic anions at 25 °C. The colour code is given at the side of the colour plots.

In Fig. 4, it can be seen that the MBA/IPA- and MPPA/IPA-selectivity are quite similar, i.e., all anion-cation combinations show a higher affinity towards MBA and MPPA. This result seems logical, as IPA has a much higher affinity for the aqueous phase, which follows from its low activity coefficient in water (γ^{∞}_{IPA} = 4.9), while MBA and MPPA show much less interaction with the aqueous phase (γ^{∞}_{MBA} = 76.2, γ^{∞}_{MPPA} = 240.1). Thus, MBA and MPPA preferentially transfer to the organic phase. Comparing the different types of anions, it seems that they all show similar trends for the MPPA/IPA-selectivity. The [FSI]- and [PF6]-based ILs, on the other hand, seem to have a higher MBA-affinity than the other anions. There is, however, also a significant effect of the cation structure on the selectivity. It seems that the phosphonium-based cations show a favourable selectivity towards MBA and MPPA with values ranging between 9–17 and 34–45, respectively. Ammonium-based anions also show high selectivity values, except for anions with shorter alkyl chains (such as propylammonium, dimethylammonium, etc.). Similarly for imidazolium-based anions, the longer the alkyl chains in the anion, the higher the selectivity values, due to the increased hydrophobicity [41]. Smaller anions, such as betaine and choline, show the lowest selectivity values.

Based on Fig. 4, fourteen cation–anion combinations have been selected to evaluate the effect of the cation and anion structure on the separation performance, as listed in Table 1. The simulated selectivity of these ILs is presented in Fig. 5. Four anions, namely $[C(CN)3]^-$, $[N(Tf)2]^-$, $[PF6]^-$ and $[BETI]^-$, and eleven cations, of which mostly are imidazolium-based cations, were selected for the experimental validation. This choice was made as these cations have the highest commercial availability, while still showing a high hydrophobicity and favourable selectivity.

3.1.2. Density calculation

To allow for a rational extractant selection, COSMO-RS was used to determine critical solvent properties *ab initio* for fourteen RTILs with varying cations and anions, as listed in Table 1. First, density calculations were performed and compared to experimental data. An ion-pair was used as the molecular geometry in COSMO-RS for density predictions. As can be seen from Fig. 6 and Fig. 7, the predictions are highly accurate with an RMSE of 0.039. Furthermore, an excellent linear fit was found between the simulated and experimental data with a linear regression coefficient R of 0.9999 and a slope of 0.9703 (see SD-4.1 in the Supplementary Information). From Fig. 6, it follows that the anion has the main effect on the IL-density, which increases in the following ranking $[C(CN)3]^- < [PF6]^- < [N(Tf)2]^- < [BETI]^-$ with a fixed [C4mim]-cation. A similar result was obtained by Troncoso et al. [42] for imidazolium-based cations combined with $[PF6]^-$ and $[N(Tf)2]^-$. It could be inferred that the IL-density often increases with the anion molecular weight, although this is not a general rule, as pointed out by Palomar et al. [43].

From Fig. 7, it can be seen that the cation structure affects the IL-density much less than the anion. All ILs have a density in the range 1.37–1.51 g/mL, except for [P6,6,6,14][N(Tf)2] which has a much lower density of 1.07 g/mL. This result is most likely linked to the longer alkyl chains of the cation, which impairs a compact packing of the molecules. Furthermore, the presence of a longer alkyl chain length in the cation decreases the IL-density, which is the case for both the imidazolium- and pyridinium-based cations. More specifically, if the cation is changed from $[C4mim]^+$ to $[C6mim]^+$ or $[C3mpy]^+$ to $[C4mpy]^+$, the density decreases. This result is in agreement with literature data [43,44]. Opposed to Fig. 6, an increase in the IL-density could not be linked with the molecular weight of the cation. Therefore, the intermolecular interactions must be determinant for volumetric properties, such as the IL-density [43].

3.1.3. Viscosity calculation

In addition to the density calculation, COSMO-RS was also used to estimate the viscosity of the selected ILs. The viscosity is a measure of the internal flow resistance of a fluid, which results from momentum transfer between the fluid's molecules across a velocity gradient. This is controlled by the fluids internal frictional forces and thus by various intermolecular interactions, such as hydrogen bonding, repulsion and short-range (i.e. van der Waals interactions) and long-range electrostatic forces [45]. The experimental and simulated viscosity results are presented in Fig. 8 and Fig. 9. Opposed to the very accurate density calculations, the viscosity is predicted much less well with an RMSE of 42.72. However, this is mostly due to the outlier of the IL [P6,6,6,14][N(Tf)2], for which the experimental and simulated viscosity equals 297.50 and 460.45 mPa s, respectively. By excluding the outlier, the RMSE decreases to 17.68 and a good linear fit between the predicted and experimental viscosity is obtained with a linear regression coefficient R of 0.9655 and a slope of 0.9016 (see SD-4.1 in the Supplementary Information).

From Fig. 8, it follows that the viscosity increases strongly within the sequence $[C(CN)3]^- < [N(Tf)2]^- < [BETI]^- < [PF6]^-$ with a fixed cation. It seems that the anion has again the largest influence on the IL-viscosity. By changing the anion from $[N(Tf)2]^-$ to $[PF6]^-$ for [C4mim]-based ionic liquids, the viscosity increased from 35.88 to 345.1 mPa s at 30 °C, according to Yadav et al. [46]. Carvalho et al [47] investigated the density and viscosity change of [C4mim]-based ILs with the $[N(CN)2]^-$ and $[C(CN)3]^-$anion and

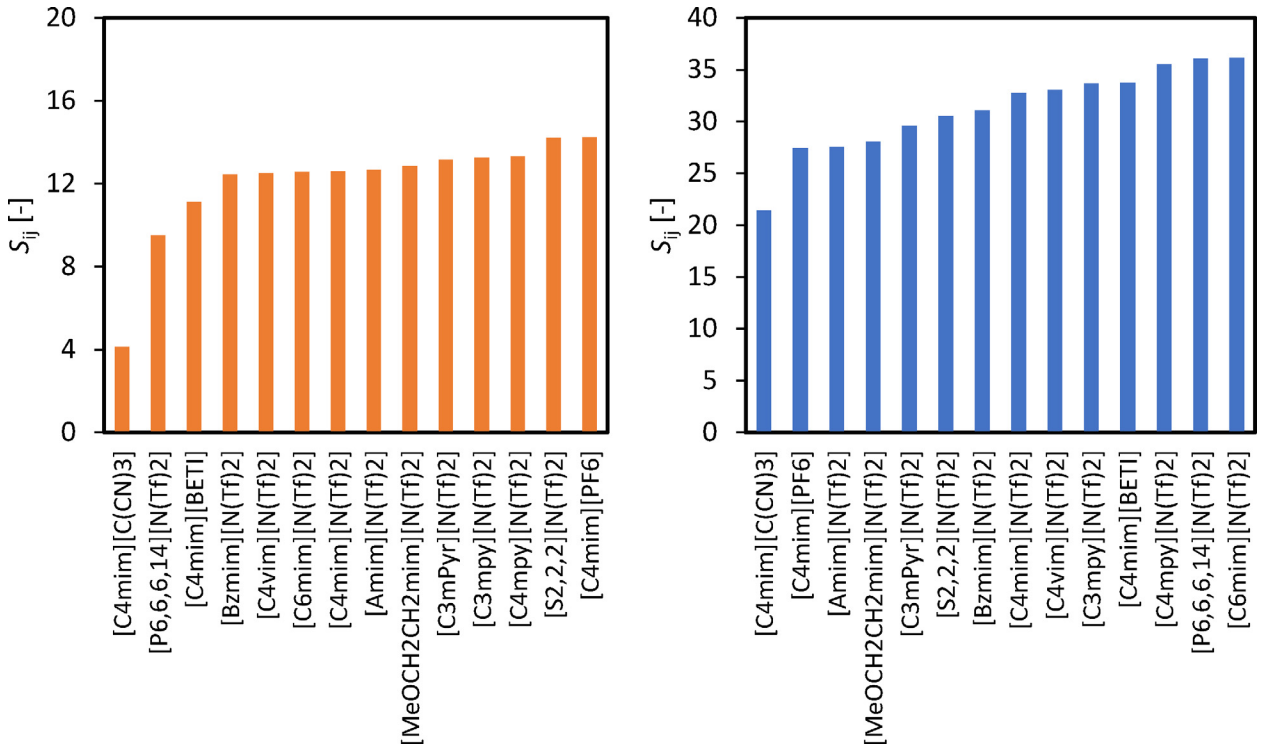

Fig. 5. Simulated selectivity of MBA (left) and MPPA (right) over IPA of various RTILs at 25 °C.

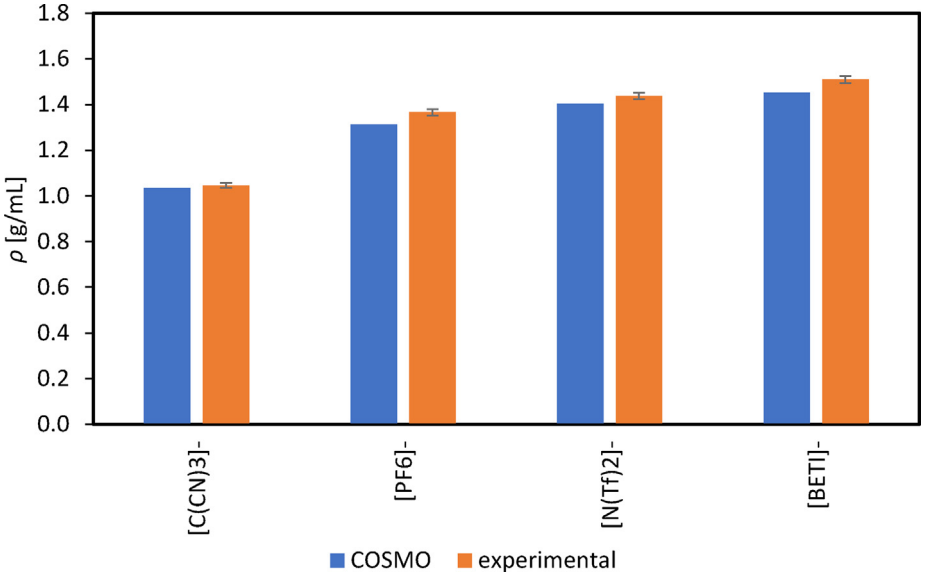

Fig. 6. Density of ILs with various anions and a common cation $[C4mim]^+$ at 30 °C.

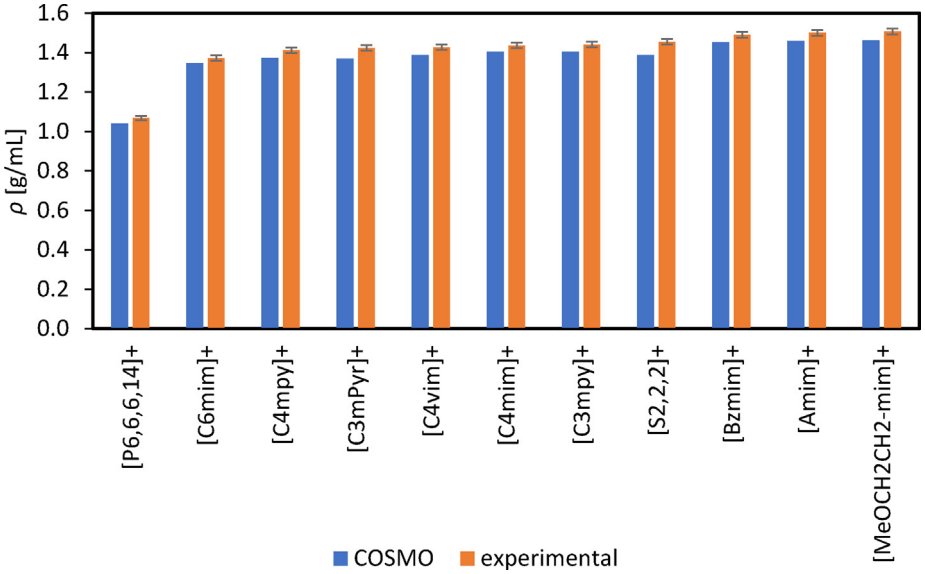

Fig. 7. Density of ILs with various cations and a common anion $[N(Tf)2]^-$ at 30 °C.

found that the viscosity was as low as 26.3 and 22.6 mPa s, respectively, which is in line with the viscosity results in this work. It seems that COSMO-RS can qualitatively predict the viscosities of the various ILs for varying anions.

The cation effect on the viscosity seems to be less pronounced than the anion effect, unless the cation consists of long, bulky alkyl chains (e.g., [P6,6,6,14]) for which a very high viscosity is observed. A similar result was obtained by Neves et al. [48], who studied the thermophysical properties of pure and water-saturated [P6,6,6,14]-based ILs. Furthermore, Verma et al. [45] noted that the viscosity increases for pyridinium-based cations with a common [N(Tf)2]-anion for longer alkyl chains. This is also seen in Fig. 9 in which the viscosity is higher for the pyridinium-based cation with a butyl chain instead of a propyl chain (i.e., from $[C3mpy]^+$ to $[C4mpy]^+$). A similar viscosity increase is observed for the imidazolium-based cations, if the cation chain length changes from four to six carbon atoms (i.e., from $[C4mim]^+$ to $[C6mim]^+$). It can be stated that COSMO-RS provides qualitative trends of the IL-viscosity, but it should be used to obtain only a first approach to quantitative viscosity data.

3.1.4. Phase miscibility calculation

The lack of large-scale SLM-applications is mainly due to the low membrane stability [49]. Various mechanisms have been proposed to explain this lack of stability, amongst others, dissolution of the solvent into the adjacent phases. As the feed and strip solution in this work are both aqueous phases, the ionic liquid to be used should have a low water miscibility to improve the SLM-stability and performance. In addition to the experimental analysis of the phase miscibility, COSMO-RS was used to simulate this property by estimating the liquid–liquid phase behaviour in the COSMOtherm program.

The water-in-IL solubility is presented in Fig. 10 and Fig. 11 for varying anions and cations, respectively. From these figures, it is clear that COSMO-RS provides a fair description of the water-in-IL solubility for most ILs. Only for the hydrophilic [C(CN)3]-anion,

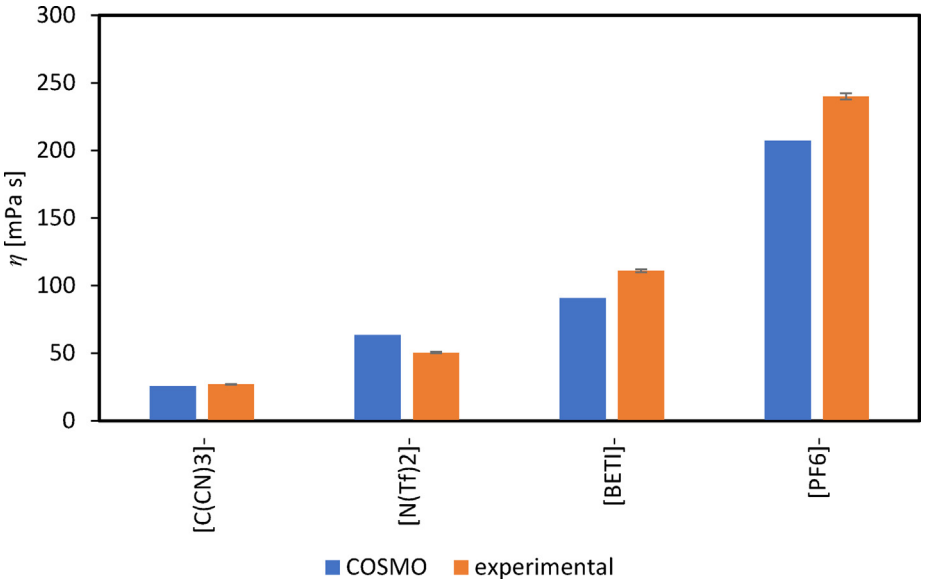

Fig. 8. Viscosity of ILs with various anions and a common cation $[C4mim]^+$ at 30 °C.

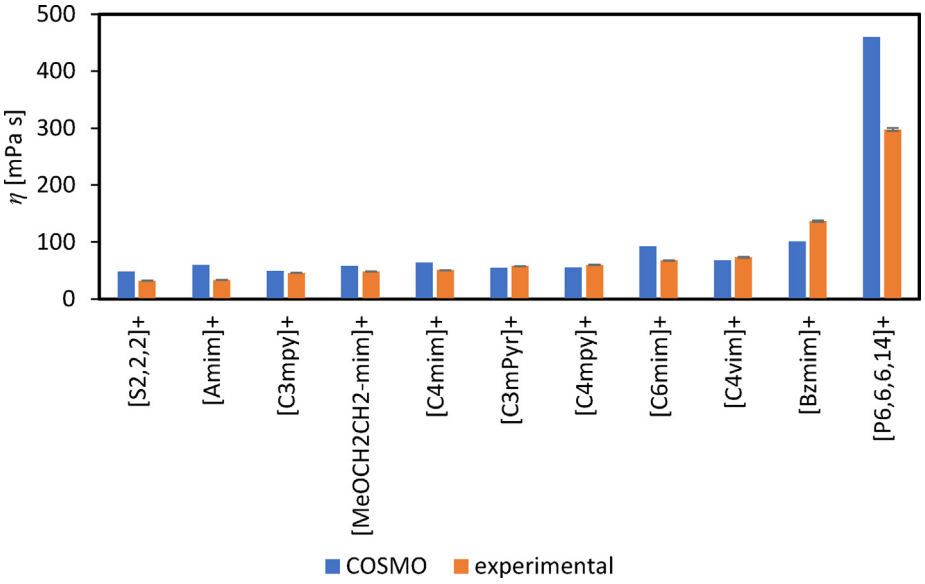

Fig. 9. Viscosity of ILs with various cations and a common anion $[N(Tf)2]^-$ at 30 °C.

COSMO-RS overpredicts the water-in-IL solubility by a factor three (i.e., 75.6 instead of 24.99 wt%). Additionally, the IL-in-water solubility is presented in Fig. 12 and Fig. 13 for varying anions and cations, respectively. Again, a fair description of the IL-in-water solubility seems to be obtained with an overprediction of the solubilities for all ILs with the exception of [P6,6,6,14][N(Tf)2], for which COSMO-RS predicts no solubility of the ionic liquid in the aqueous phases. The overall miscibility range of the considered ILs can be found in SD-4.2 in the Supplementary Information.

Freire et al. [50,51] indicated that the major deviations of the phase miscibility predictions occur for small-sized anions with a higher charge density, such as bromide and chloride. This can be linked to the charge distribution on the molecular surface of the ILs, which can be visualized by COSMO-RS using the σ-profile. These profiles can be used to estimate possible interactions of compounds in a fluid. A σ-profile can be divided in three regions, namely a hydrogen bond donor ($\sigma < -0.01$ e/Å^2) and acceptor region ($\sigma > 0.01$ e/Å^2), and a nonpolar region ($-0.01 < \sigma < 0.01$ e/Å^2) [33]. The σ-profiles of the considered cations, anions and anion-cation combinations is given in SD-5, SD-6 and SD-7 in the Supplementary Information, respectively. From the σ-profiles of the considered anions, it can be seen that the [Cl]-anion is situated in the basic region, while the other anions (i.e., $[PF6]^-$, $[C(CN)3]^-$, $[N(Tf)2]^-$ and $[BETI]^-$) mostly show peaks in the neutral region. The σ-profile of the [C(CN)3]-anion is mainly located on the positive side with values passing 0.01 e/Å^2, indicating the tendency of the nitrogen atoms of $[C(CN)3]^-$ to accept hydrogen bonds in water [52]. While the [N(Tf)2]- and [BETI]-anion show a similar σ-profile (with larger peaks), their basic behaviour is less pronounced. This is also observed by Cláudio et al. [38], who found that the [C(CN)3]-anion has the highest hydrogen bond basicity of the considered anions in this study. This could also explain the strong overprediction of the water-in-IL and IL-in-water solubility for this anion. For both the water-in-IL and IL-in-water solubility,

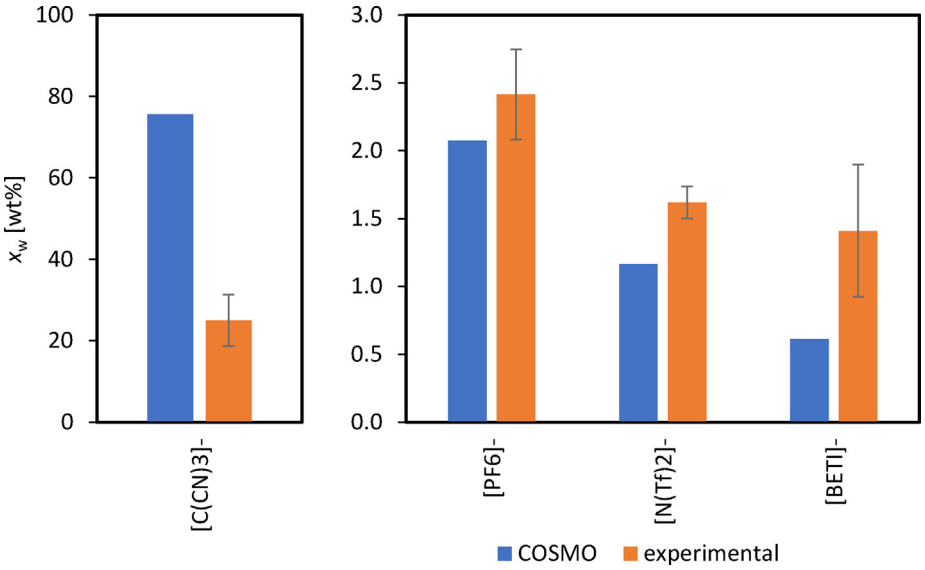

Fig. 10. Water solubility in ILs with various anions and a common cation $[C4mim]^+$ at 30 °C.

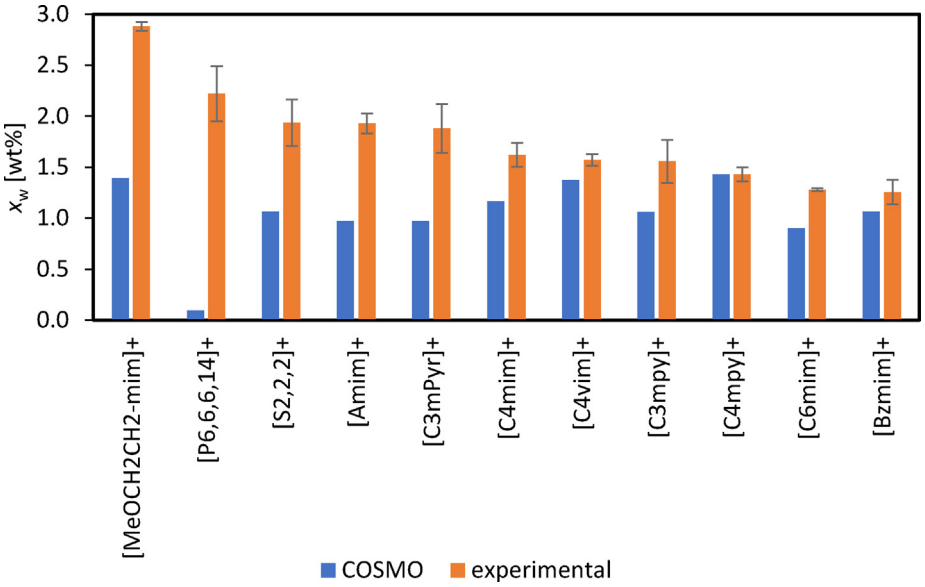

Fig. 11. Water solubility in ILs with various cations and a common anion $[N(Tf)2]^-$ at 30 °C.

COSMO-RS predicts the following trend in order of decreasing solubility in the other phase: $[C(CN)3]^- < [PF6]^- < [N(Tf)2]^- < [BETI]^-$. This trend is also observed experimentally for the water-in-IL solubility, but no large differences are observed experimentally between the [PF6]-, [N(Tf)2]- and [BETI]-anion for the IL-in-water solubility. It could be stated that COSMO-RS can qualitatively predict the water-in-IL solubility for varying anions.

On the other hand, no satisfactory results were obtained for the water-in-IL and IL-in-water solubility predictions for varying cation structures With exception of the outlier [P6,6,6,14][N(Tf)2], it seems that COSMO-RS predicts a very similar water-in-IL solubility for all cations in the range of 0.90 – 1.43 wt%, whilst the IL-in-water solubility shows a larger variation between 1.67 and 7.84 wt%.

3.2. Solvent and support selection

After prediction of the density, viscosity and phase miscibility of the solvent using COSMO-RS, a selection of shortlist candidates is made, based on experimental testing of the selectivity and extraction efficiency of various ionic liquids. Next, the wettability of various support materials was tested in order to select the most appropriate membrane.

3.2.1. Solvent selection

To design a contactor using SLM for the separation of chiral amines, a suitable solvent needs to be selected first. To this end, liquid–liquid extraction experiments were performed to compare the solvent performance and selectivity for the extraction of MBA, MPPA and IPA. A shortlist of four promising ionic liquids was made, including [S2,2,2][N(Tf)2], [C3mPyr][N(Tf)2], [C6mim][N(Tf)2] and [P6,6,6,14][N(Tf)2]. More specifically, the ionic liquids [C6mim][N(Tf)2] and [P6,6,6,14][N(Tf)2] were selected, because they showed a high MPPA/IPA-selectivity of 36.2 and 36.1, respectively (see Fig. 5). On the other hand, [S2,2,2][N(Tf)2] was selected as it had the highest MBA/IPA-selectivity of 14.2 (see Fig. 5), apart from [C4mim][PF6], which was not chosen due to its instability in

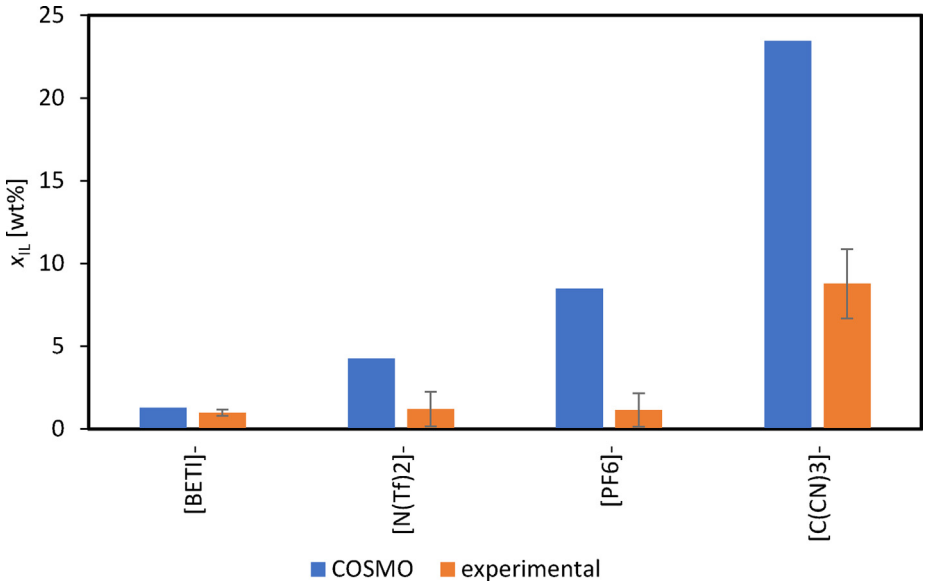

Fig. 12. Ionic liquid solubility in water for ionic liquids with various anions and a common cation $[C4mim]^+$ at 30 °C.

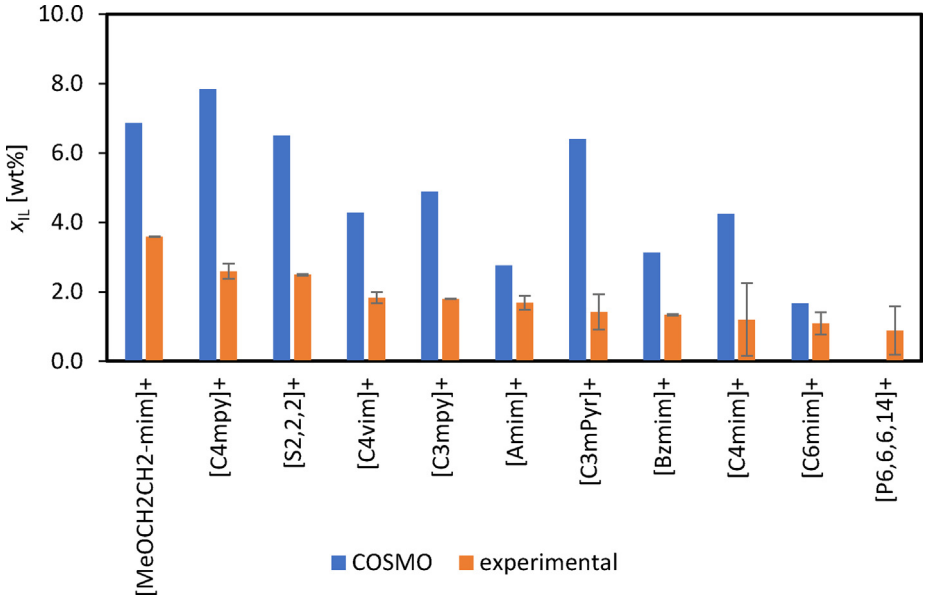

Fig. 13. Ionic liquid solubility in water for ionic liquids with various cations and a common anion $[N(Tf)2]^-$ at 30 °C.

aqueous phases [39]. To address the cation effect, [C3mPyr][N(Tf)2] was also chosen to include a pyrrolidinium cation in the study. Finally, Aliquat-336 was selected as the benchmarking solvent, as this is a conventionally used ionic liquid for extraction applications in the literature, such as metal ion recovery [53] and wastewater treatment [54].

The extraction results are plotted in Fig. 14. All ionic liquids have a very high MPPA-extraction efficiency of>0.90. The MBA-extraction performance, on the other hand, is much lower for [C6mim][N(Tf)2] and [P6,6,6,14][N(Tf)2], namely 0.795 and 0.596, respectively. The IPA-extraction is also much lower for these ionic liquids at values of 0.072 and 0.031, respectively, compared to values above 0.15 for the others. This can be linked to the selectivity values for all ionic liquids, which are plotted in Fig. 15. Despite the lower MBA- and MPPA-extraction, [P6,6,6,14][N(Tf)2] shows the highest selectivity, making it the most promising IL-candidate for this separation. It should be noted that COSMO-RS predicted a higher affinity of all ILs for MPPA compared to MBA, which can be explained by the σ-profiles of the different solutes, as presented in SD-8 in the Supplementary Information. MBA and MPPA are both quite nonpolar compounds with peaks covering the complete neutral region ($-0.01 \leq \sigma \leq 0.01$). MBA shows less pronounced peaks than MPPA, which makes MBA slightly more polar than MPPA. Furthermore, the simulated activity coefficients of MBA and MPPA in the aqueous phase were 76.2 and 240.1, respectively. Thus, MBA seems to be more likely to remain in the aqueous phase than MPPA. This was also observed experimentally, as MPPA was extracted more than MBA for all the ILs. The experimental solubility values of MBA and MPPA, i.e., 42,000 and 12,000 mg/L further support these results, as MBA is more soluble in water than MPPA [55].

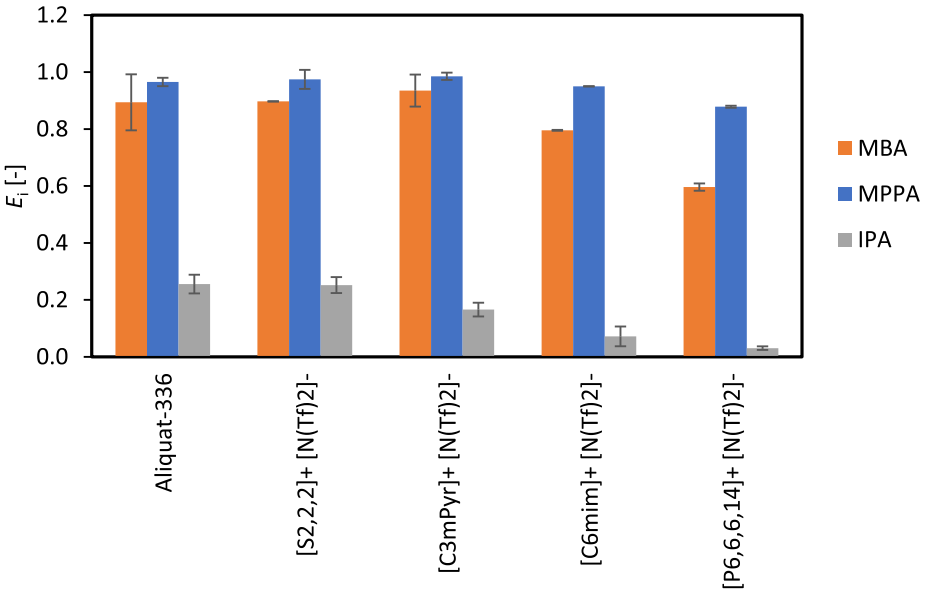

Fig. 14. Experimental extraction efficiency of four RTILs for the separation of MBA and MPPA from IPA, compared with Aliquat-336.

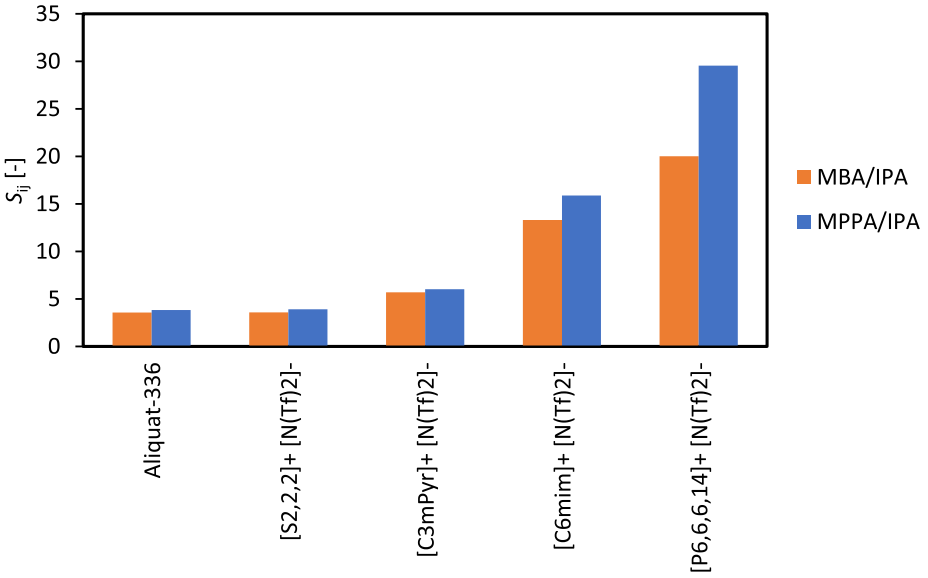

Fig. 15. Experimental selectivity of four RTILs for the separation of MBA and MPPA from IPA, compared with Aliquat-336.

3.2.2. Support selection

Four different porous membranes were chosen as possible supports, namely polytetrafluoroethylene (PTFE), polyethersulfone (PES), polysulfone (PSf) and polyvinylidene fluoride (PVDF) with an average pore size as listed in Table 2. The PTFE-membrane with a pore size of 100 nm and polypropylene support was used for the contact angle measurements. To determine the wettability of the support materials with the ionic liquid phase, the static contact angle was measured as explained in Section 2.2. The wettability results of the considered ILs are given in Fig. 16 and Fig. 17 and compared to the static water contact angle. All the support materials show a better wettability of the organic IL-phase compared to water. Furthermore, PTFE shows the highest contact angle for both water and the IL-phases, compared to PES, PSf and PVDF. No large differences seem to be present between the PES-, PSf- and PVDF-support, as follows from the box plot analysis in SD-9 in the Supplementary Information. Despite the lower IL-wettability of the PTFE-support, this material was chosen for the ME-testing, as it shows the highest water contact angle to avoid pore wetting by the aqueous phases.

Pereira et al. [40] studied the wettability of various ILs on both polar (glass, aluminium) and nonpolar (PTFE) surfaces. They found that the hydrogen-bond basicity of the ILs, which is closely related to the anion structure, has a significant effect on the wettability. If the IL-basicity increases, the IL shows an improved wettability on more polar surfaces, while the opposite trend is observed for nonpolar surfaces. The basicity scale as presented by Cláudio et al. [38] gives the following ranking of the anions for a decreasing hydrogen-bonding interaction energy: $[C(CN)3]^- < [N(Tf)2]^- < [BETI]^- < [PF6]^-$. The results in this study follow the same ranking for the wetting on the nonpolar PTFE-surface, except for the [PF6]-anion, which should show the most favourable wettability, based on this basicity scale. Contrary to the anion effect, Pereira et al. [40] stated that the cation structure (such as the alkyl side

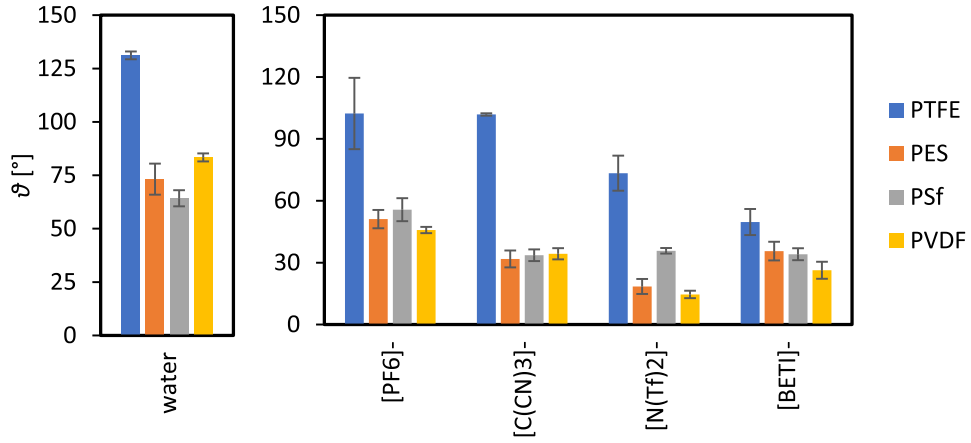

Fig. 16. Contact angle of water (left) and ILs with various anions and a common cation $[C4mim]^+$ (right) on four polymeric porous substrates.

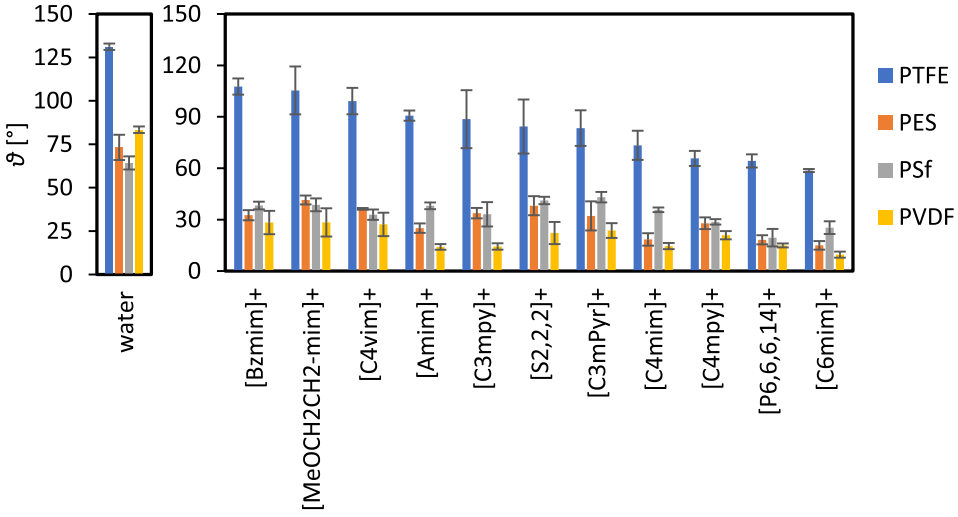

Fig. 17. Contact angle of water (left) and ILs with various cations and a common anion $[N(Tf)2]^-$ (right) on four polymeric porous substrates.

chain length) and nature have a smaller impact on the IL-wettability. Interestingly, in this study the anion and cation seem to affect the wettability behaviour to a similar degree (see SD-9 in the Supplementary Information). This is most likely due to the fact that the study of Pereira et al. [40] focussed on imidazolium-based cations with various alkyl chain lengths, which influence the hydrophobicity less. The cations studied in this work also contained more polar side groups, such as ether and alkene groups, and the more nonpolar [S2,2,2]- and [P6,6,6,14]-cations, which could explain the larger variability.

The comparison of wetting data with the literature is difficult due to the lack of values for the same supports, which was also noted by Pereira et al. [40]. For example, the result in this study for [C4mim][PF6] (i.e., 102.3°) is significantly different from the literature value (i.e., 60.11°). The main factor which causes variations in the results might be the non-porosity of the used substrates in literature, whilst in this study porous materials were used, for which the wetting profile (as indicated in the Supplementary Information) is different compared to non-porous substrates. Additionally, [PF6]-anions are unstable in the presence of water and suffer from hydrolysis, which could cause an impaired wetting, despite the fluorinated nature of the [PF6]-anion.

3.3. SLM-performance

3.3.1. SLM-stability

The four ionic liquids selected in Section 3.2.1 were used to perform stability tests, which were performed similarly to the membrane extraction tests, except that no amines were added to the feed solution. The feed and strip were circulated counter-currently through the membrane contactor, until the membrane failed, i.e., a clear volume difference was visible between the feed and strip phase, or the experiment was stopped after 24 h. In some cases, e.g., for Aliquat-336, the membrane already failed after less than one hour. The results are presented in Fig. 18, showing that all the ionic liquids with the exception of [P6,6,6,14][N(Tf)2] are very unstable in the membrane contactor. Furthermore, despite the high residual solvent mass of undecane in the membrane pores, this solvent shows a very large variation, indicating its sensitivity towards small variations in operating conditions. The tests with undecane were also prone to failure, i.e., volume loss from the feed to the strip or vice versa, which indicates the formation of water channels through the membrane. The only extractant showing a desirable stability was [P6,6,6,14][N(Tf)2] with an average residual solvent mass of 101.1 % and a small standard deviation of 2.5 %.

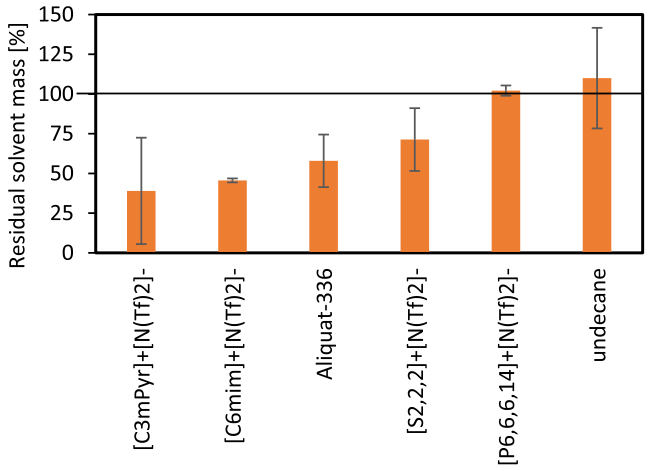

Fig. 18. Solvent mass remaining in the membrane after a stability test for four RTILs for the separation of MBA and MPPA from IPA, compared with Aliquat-336 and undecane.

Slight increases in the solvent mass (i.e., a residual solvent mass>100 %) might be due to water absorption by the extractant.

The stability of supported liquid membranes is influenced by a variety of factors. One of the main factors causing SLM-instability is the formation of stable emulsions between the LM-phase and the adjacent phases, according to Neplenbroek et al. [56]. More specifically, they hypothesised that local deformations of the liquid meniscus in the membrane pores may cause the splitting off and formation of emulsion droplets. These deformations may originate from the shear flow of the feed and strip phase (referred to as Kelvin-Helmholz instabilities) or membrane vibrations. They also stated that no clear correlation was found between the SLM-stability and other physical parameters, such as the interfacial tension, salt content and molecular solubility. Furthermore, the presence of an osmotic pressure difference did not seem to affect the SLM-instability. Xu et al. [57] found that solvent leakage could be reduced by changing the acidity of the adjacent aqueous phases. Koonsang et al. [58] and Seip et al. [59] also noted the influence of the feed and strip pH on the SLM-stability, next to other solvent properties, such as the water solubility, molecular surface area, log *P* value, dipole moment and basicity of the LM-phase. Additionally, the SLM-stability can be prolonged by enhancing the hydrophobicity of the SLM-support phase [60,61].

Different parameters, i.e., viscosity, water solubility, hydrophobicity and emulsification, were analysed to elucidate the causes of the SLM-instability. These properties, except for the emulsion formation, are listed in Table 3. It could be stated that the water solubility is not the main factor, as all the tested ILs show a water solubility in the same range (1.3 – 2.2 wt%), except for Aliquat-336 (18.2 wt%), which could explain its low SLM-stability. The hydrophobicity can be estimated by the Hansen Solubility Parameters (HSP), which are split into three contributions due to dispersive (δ_D), polar (δ_P) and hydrogen bonding (δ_H) interactions. Undecane is clearly the most hydrophobic solvent, as it only shows dispersive interactions. For the ILs, on the other hand, [P6,6,6,14][N(Tf)2] seems to be the most hydrophobic showing the least polar and hydrogen bonding interactions. It should be noted that no large differences are found between the considered ILs, which all show very similar solubilities (see SD-10 in the Supplementary Information). As stated by Neplenbroek et al. [56], the emulsion stability is an important factor affecting the SLM-stability. The emulsion stability can be linked to the demulsification speed, which is given qualitatively in SD-11 in the Supplementary Information. However, no clear correlations could be found for the ILs studied in this work. Surprisingly, the unstable ILs [C3mPyr][N(Tf)2] and [S2,2,2][N(Tf)2] did not show any emulsification after ultrasonication, which would imply a higher stability. From SD-11, it follows that undecane shows the fastest demulsification, whilst Aliquat-336 gives the most stable emulsion, which is in line with the results of Neplenbroek et al. [56]. However, [P6,6,6,14][N(Tf)2] and [C6mim][N(Tf)2] show a similar demulsification speed, whilst the latter is considered as unstable when compared to the former. Therefore, emulsion stability does not seem to be the main influence on the SLM-stability. The final parameter considered was the viscosity, which is the lowest for undecane and the highest for [P6,6,6,14][N(Tf2], as presented in Table 3. Based on the results in this work, it seems that the viscosity is the main factor on SLM-stability, i.e., a higher viscosity leads to an improved SLM-stability. However, Aliquat-336 showed quite a low stability, while having a viscosity of 1655.6 mPa s. Next to having a high viscosity, the solvent should be water-insoluble and hydrophobic to prevent wetting and solubilisation of the LM-phase into the adjacent phases.

3.3.2. SLM-extraction performance

Based on the property analysis and stability tests, the ionic liquid [P6,6,6,14][N(Tf)2] was chosen as the optimal extractant for the separation of chiral amines. As mentioned before, the SLM should show a higher selectivity towards the product amines MBA and MPPA compared to the donor amine IPA. Based on a difference in solubility and affinity, the chosen LM-phase will extract MBA and MPPA more than IPA. As mentioned by Rehn et al. [19,20], an alkaline feed buffer and acidic strip buffer were used at a pH of 10 and 3, respectively. The lower strip pH is required to prevent back-extraction into the LM-phase, as the protonated amines cannot re-enter from the stripping phase. An important note is that for the SLM-tests a PTFE-support was used with a pore size of 50 nm instead of 100 nm, as a lower pore size improves the stability even further [21].

The SLM-extraction results of [P6,6,6,14][N(Tf)2] at different temperatures are given in Fig. 19, next to the benchmark undecane. The flux definition and calculation procedure is described in SD-12 in the Supplementary information. The selectivity is defined as the ratio of the MBA- or MPPA-flux and the IPA-flux. From Fig. 19 (a), a difference between the feed and strip flux can be observed. More specifically, the solute flux from the LM-phase to the strip is slightly lower than the solute flux from the feed to the LM-phase for MBA and MPPA. For IPA, the strip flux is much lower compared

Table 3
Properties of the shortlist ionic liquid candidates.

Solvent	η mPa s	x_w wt%	δ_D MPa$^{1/2}$	δ_P MPa$^{1/2}$	δ_H MPa$^{1/2}$	Ref.
Undecane	1.098	< 0.1	16.0	0	0	[62,63]
[C3mPyr][N(Tf)2]	57.7	1.9	17.1	12.9	14.1	This work
[C6mim][N(Tf)2]	67.8	1.3	16.9	13.5	14.4	This work
[S2,2,2][N(Tf)2]	32.3	1.9	16.9	13.5	14.4	This work
[P6,6,6,14][N(Tf)2]	297.5	2.2	17.2	12.1	13.6	This work

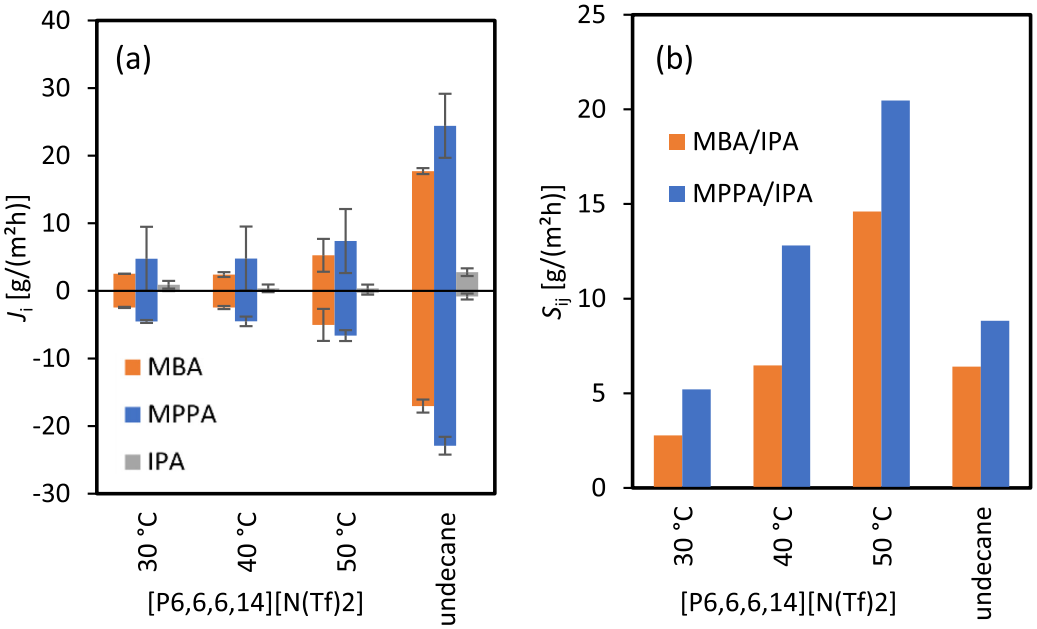

Fig. 19. (a) Averaged solute fluxes of the feed and strip phase, indicated by positive and negative values, respectively; and (b) selectivity for the SLM-extraction of MBA and MPPA over IPA. The SLM-results are given at a temperature of 30, 40 and 50 °C for the ionic liquid [P6,6,6,14][N(Tf)2], compared with undecane at 30 °C.

to the feed flux. This indicates that MBA and MPPA are extracted preferentially to the LM-phase and the strip phase, whilst IPA remains mostly in the feed phase. Additionally, the IPA which is extracted into the LM-phase remains mostly there, due to its higher affinity for this phase, compared to MBA and MPPA, which is also reflected in their activity coefficients ($\gamma_{MBA} = 1.175$, $\gamma_{MPPA} = 0.975$, $\gamma_{IPA} = 0.712$). As IPA shows the lowest γ^{∞}, it has the highest affinity for the LM-phase.

Fig. 19 (a) shows that undecane has larger fluxes for MBA, MPPA and IPA, compared to the chosen ionic liquid. The lower viscosity may cause this difference in fluxes. By increasing the temperature, the MBA- and MPPA-flux of [P6,6,6,14][N(Tf)2] increase significantly, whilst the IPA-flux remains at a much lower value. The improved fluxes could be due to a decreased viscosity of the LM-phase, which decreases from 216.8 to 82.9 mPa s at 30 and 50 °C, respectively (see SD-13 in the Supplementary Information). In addition, the IPA-flux for the ionic liquid is much lower compared to undecane for all the studied temperatures. This results in a much higher IL-selectivity, especially at an elevated temperature of 50 °C, as presented in Fig. 19 (b). Based on these results, it is clear that the ionic liquid [P6,6,6,14][N(Tf)2] provides an interesting alternative to the conventional extractant undecane, due to its much higher selectivity.

4. Conclusion

In this work, a solvent screening was performed to determine the optimal extractant for the supported liquid membrane (SLM) extraction of chiral amines, i.e., α methylbenzylamine (MBA), 1-methyl-3-phenylpropylamine (MPPA) and isopropyl amine. To this end, the MBA/IPA- and MPPA/IPA-selectivity of up to 400 different anion-cation combinations were determined, which showed that the anions $[FSI]^-$ and $[PF6]^-$ are those with a more favourable interaction with the chiral amines. The molecular structure of the cation also has a significant impact on the selectivity, with phosphonium- and ammonium-based cations being the most suitable candidates. As the alkyl chains of the cation increase in length, the selectivity becomes higher. Similarly, smaller anions have a negative effect on the selectivity. Based on these results, fourteen ionic liquids (ILs) were selected in this work to analyse their critical solvent properties experimentally and via COSMO-RS simulations. COSMO-RS gave excellent density (RMSE = 0.039) and satisfactory viscosity (RMSE = 44.19) predictions. For varying anions, COSMO-RS gave qualitative trends of the water-in-IL solubility x_w, whilst x_w was underpredicted when varying the cation structure. The IL-in-water solubility x_{IL}, on the other hand, was overpredicted for all ILs, except for [P6,6,6,14][N(Tf)2]. Hence, COSMO-RS should only be used for rough quantitative descriptions of x_w and x_{IL} of ionic liquids. The performance of the four most promising solvents was tested in conventional liquid–liquid extraction tests, which showed that all ILs show a higher affinity towards MBA and MPPA, as predicted by COSMO-RS. The IL [P6,6,6,14][N(Tf)2] showed the highest selectivity for the separation application at hand. After solvent selection, the wettability of four different polymeric substrates (PTFE, PES, PSf, PVDF) was tested. From these tests, it follows that PTFE showed the least favourable IL-wettability due to its very high hydrophobicity. Due to the high water contact angle, the PTFE-substrate was chosen for the SLM-extraction tests. The four selected ILs were immobilised in the porous PTFE-membrane to prepare the SLMs and test their stability. The main factors influencing the stability seem to be the water solubility x_w and viscosity η. More specifically, a lower x_w and higher η enhance the stability, as the most viscous IL [P6,6,6,14][N(Tf)2] showed the highest stability. The temperature had a strong influence on the SLM-performance, i.e., an increase in the temperature improved the solute fluxes and selectivity, which could be attributed to a decrease in the IL-viscosity. In conclusion, the current work proposes an extraction process using supported ionic liquid membranes for the separation of chiral amines. The use of ionic liquids as alternative extractants seems to be a promising route to follow, as they provide a higher selectivity and stability, compared to the organic solvents conventionally used in literature.

Data availability

Data will be made available on request.

Declaration of Competing Interest

The authors declare that they have no known competing financial interests or personal relationships that could have appeared to influence the work reported in this paper.

Acknowledgements

The authors would like to thank the support of the Flemish Strategic Basic Research Program of the Catalisti cluster and Flanders Innovation & Entrepreneurship in the framework of the EASi-CHEM project (contracts HBC.2018.0484 and K200522N). This work was partly developed within the scope of the project CICECO-Aveiro Institute of Materials, UIDB/50011/2020, UIDP/50011/2020 & LA/P/0006/2020, financed by national funds through the FCT/MEC (PIDDAC). Additionally, the authors would like to thank Stijn Keuppens, Lander De Geest and Rick Steenmans for their aid in the experimental part of this paper.

Appendix A. Supplementary material

Supplementary data to this article can be found online at https://doi.org/10.1016/j.molliq.2023.121351.

References

[1] F. Mutti, Molecular science: The importance of sustainable manufacturing of chiral amines, 2020. https://www.openaccessgovernment.org/chiral-amines/52451/.
[2] D. Ghislieri et al., Engineering an enantioselective amine oxidase for the synthesis of pharmaceutical building blocks and alkaloid natural products, J. Am. Chem. Soc. 135 (29) (2013) 10863–10869, https://doi.org/10.1021/ja4051235.
[3] D. Koszelewski, I. Lavandera, D. Clay, D. Rozzell, W. Kroutil, Asymmetric synthesis of optically pure pharmacologically relevant amines employing ω-transaminases, Adv. Synth. Catal. 350 (17) (2008) 2761–2766, https://doi.org/10.1002/adsc.200800496.
[4] Y. Bandala, E. Juaristi, Recent Advances in the Application of α-Phenylethylamine (α-PEA) in the Preparation of Enantiopure Compounds, Aldrichim. Acta 43 (3) (2010) 65–78.
[5] T.C. Nugent, M. El-Shazly, Chiral amine synthesis - Recent developments and trends for enamide reduction, reductive amination, and imine reduction, Adv. Synth. Catal. 352 (5) (2010) 753–819, https://doi.org/10.1002/adsc.200900719.
[6] C.K. Savile et al., Biocatalytic Asymmetric Synthesis of Sitagliptin Manufacture, Science (80-.) 329 (July) (2010) 305–310, https://doi.org/10.1126/science.1188934.
[7] P. Stockinger et al., Inverting the Stereoselectivity of an NADH-Dependent Imine-Reductase Variant, ChemCatChem 13 (24) (2021) 5210–5215, https://doi.org/10.1002/cctc.202101057.
[8] P. Kelefiotis-Stratidakis, T. Tyrikos-Ergas, I.V. Pavlidis, The challenge of using isopropylamine as an amine donor in transaminase catalysed reactions, Org. Biomol. Chem. 17 (7) (2019) 1634–1642, https://doi.org/10.1039/c8ob02342e.
[9] K.S. Hayes, Industrial processes for manufacturing amines, Appl. Catal. A Gen. 221 (1–2) (2001) 187–195, https://doi.org/10.1016/S0926-860X(01)00813-4.
[10] D. Koszelewski, K. Tauber, K. Faber, W. Kroutil, ω-Transaminases for the synthesis of non-racemic α-chiral primary amines, Trends Biotechnol. 28 (6) (2010) 324–332, https://doi.org/10.1016/j.tibtech.2010.03.003.
[11] P. Tufvesson, J. Lima-Ramos, J.S. Jensen, N. Al-Haque, W. Neto, J.M. Woodley, Process considerations for the asymmetric synthesis of chiral amines using transaminases, Biotechnol. Bioeng. 108 (7) (2011) 1479–1493, https://doi.org/10.1002/bit.23154.
[12] A.C. Eliot, J.F. Kirsch, Pyridoxal phosphate enzymes: Mechanistic, structural, and evolutionary considerations, Annu. Rev. Biochem. 73 (2004) 383–415, https://doi.org/10.1146/annurev.biochem.73.011303.074021.
[13] M.D. Truppo, J. David Rozzell, N.J. Turner, Efficient production of enantiomerically pure chiral amines at concentrations of 50 g/L using transaminases, Org. Process Res. Dev. 14 (1) (2010) 234–237, https://doi.org/10.1021/op900303q.
[14] M. Höhne, S. Kühl, K. Robins, U.T. Bornscheuer, Efficient asymmetric synthesis of Chiral amines by combining transaminase and pyruvate decarboxylase, ChemBioChem 9 (3) (2008) 363–365, https://doi.org/10.1002/cbic.200700601.
[15] M.D. Truppo, N.J. Turner, J.D. Rozzell, Efficient kinetic resolution of racemic amines using a transaminase in combination with an amino acid oxidase, Chem. Commun. 16 (2009) 2127–2129, https://doi.org/10.1039/b902995h.
[16] A. Iwasaki, Y. Yamada, N. Kizaki, Y. Ikenaka, J. Hasegawa, Microbial synthesis of chiral amines by (R)-specific transamination with Arthrobacter sp. KNK168, Appl. Microbiol. Biotechnol. 69 (5) (2006) 499–505, https://doi.org/10.1007/s00253-005-0002-1.
[17] A.R. Martin, R. DiSanto, I. Plotnikov, S. Kamat, D. Shonnard, S. Pannuri, Improved activity and thermostability of (S)-aminotransferase by error-prone polymerase chain reaction for the production of a chiral amine, Biochem. Eng. J. 37 (3) (2007) 246–255, https://doi.org/10.1016/j.bej.2007.05.001.
[18] G. Van Eygen, B. Van der Bruggen, A. Buekenhoudt, P. Luis Alconero, Efficient membrane-based affinity separations for chemical applications: A review, Chem. Eng. Process. - Process Intensif. 169 (Dec. 2021), https://doi.org/10.1016/j.cep.2021.108613.
[19] G. Rehn, P. Adlercreutz, C. Grey, Supported liquid membrane as a novel tool for driving the equilibrium of ω-transaminase catalyzed asymmetric synthesis, J. Biotechnol. 179 (1) (2014) 50–55, https://doi.org/10.1016/j.jbiotec.2014.03.022.
[20] G. Rehn, B. Ayres, P. Adlercreutz, C. Grey, An improved process for biocatalytic asymmetric amine synthesis by in situ product removal using a supported liquid membrane, J. Mol. Catal. B Enzym. 123 (2016) 1–7, https://doi.org/10.1016/j.molcatb.2015.10.010.
[21] Y.T. Ong, K.F. Yee, Y.K. Cheng, S.H. Tan, A review on the use and stability of supported liquid membranes in the pervaporation process, Sep. Purif. Rev. 43 (1) (2014) 62–88, https://doi.org/10.1080/15422119.2012.716134.
[22] P. Luis, I. Ortiz, R. Aldaco, A. Irabien, A novel group contribution method in the development of a QSAR for predicting the toxicity (Vibrio fischeri EC50) of ionic liquids, Ecotoxicol. Environ. Saf. 67 (3) (2007) 423–429, https://doi.org/10.1016/j.ecoenv.2006.06.010.
[23] H. Niedermeyer, J.P. Hallett, I.J. Villar-Garcia, P.A. Hunt, T. Welton, Mixtures of ionic liquids, Chem. Soc. Rev. 41 (23) (2012) 7780–7802, https://doi.org/10.1039/c2cs35177c.
[24] T. Banerjee, A. Khanna, Infinite dilution activity coefficients for trihexyltetradecyl phosphonium ionic liquids: Measurements and COSMO-RS prediction, J. Chem. Eng. Data (2006), https://doi.org/10.1021/je0602925.
[25] L. Gou et al., A hybrid process for chiral separation of compound-forming systems, Chirality (2011), https://doi.org/10.1002/chir.20886.
[26] M.A.R. Martins, U. Domańska, B. Schröder, J.A.P. Coutinho, S.P. Pinho, Selection of Ionic Liquids to be Used as Separation Agents for Terpenes and Terpenoids, ACS Sustain. Chem. Eng. (2016), https://doi.org/10.1021/acssuschemeng.5b01357.
[27] S.M. Vilas-Boas et al., Ionic liquids as entrainers for terpenes fractionation and other relevant separation problems, J. Mol. Liq. (2021), https://doi.org/10.1016/j.molliq.2020.114647.
[28] M.Z.M. Salleh, M.K. Hadj-Kali, M.A. Hashim, S. Mulyono, Ionic liquids for the separation of benzene and cyclohexane – COSMO-RS screening and experimental validation, J. Mol. Liq. (2018), https://doi.org/10.1016/j.molliq.2018.06.034.
[29] X. Zhao et al., Liquid-liquid extraction of lithium from aqueous solution using novel ionic liquid extractants via COSMO-RS and experiments, Fluid Phase Equilib. (2018), https://doi.org/10.1016/j.fluid.2017.11.038.
[30] M.K. Hadj-Kali, M. Althuluth, S. Mokraoui, I. Wazeer, E. Ali, D. Richon, Screening of ionic liquids for gas separation using COSMO-RS and comparison between performances of ionic liquids and aqueous alkanolamine solutions, Chem. Eng. Commun. (2020), https://doi.org/10.1080/00986445.2019.1680363.
[31] H.W. Khan, A.V.B. Reddy, M.M.E. Nasef, M.A. Bustam, M. Goto, M. Moniruzzaman, Screening of ionic liquids for the extraction of biologically active compounds using emulsion liquid membrane: COSMO-RS prediction and experiments, J. Mol. Liq. (2020), https://doi.org/10.1016/j.molliq.2020.113122.
[32] Z. Zhang, R. Lu, Q. Zhang, J. Chen, W. Li, COSMO-RS based ionic liquid screening for the separation of acetonitrile and ethanol azeotropic mixture, J. Chem. Technol. Biotechnol. (2020), https://doi.org/10.1002/jctb.6305.
[33] P. Arenas, I. Suárez, B. Coto, Combination of molecular dynamics simulation, COSMO-RS, and experimental study to understand extraction of naphthenic acid, Sep. Purif. Technol. 280 (August) (2021) 2022, https://doi.org/10.1016/j.seppur.2021.119810.
[34] L. Janoschek, L. Grozdev, S. Berensmeier, Membrane-assisted extraction of monoterpenes: From in silico solvent screening towards biotechnological process application, R. Soc. Open Sci. 5 (4) (2018), https://doi.org/10.1098/rsos.172004.
[35] J.P. Wojeicchowski, C. Marques, L. Igarashi-Mafra, J.A.P. Coutinho, M.R. Mafra, Extraction of phenolic compounds from rosemary using choline chloride – based Deep Eutectic Solvents, Sep. Purif. Technol. (2021), https://doi.org/10.1016/j.seppur.2020.117975.
[36] K. Paduszyński, An overview of the performance of the COSMO-RS approach in predicting the activity coefficients of molecular solutes in ionic liquids and derived properties at infinite dilution, Phys. Chem. Chem. Phys. (2017), https://doi.org/10.1039/c7cp00226b.
[37] X. Zhang et al., COSMO-based solvent selection and Aspen Plus process simulation for tar absorptive removal, Appl. Energy (2019), https://doi.org/10.1016/j.apenergy.2019.113314.
[38] A.F.M. Cláudio, L. Swift, J.P. Hallett, T. Welton, J.A.P. Coutinho, M.G. Freire, Extended scale for the hydrogen-bond basicity of ionic liquids, Phys. Chem. Chem. Phys. 16 (14) (2014) 6593–6601, https://doi.org/10.1039/c3cp55285c.
[39] P. Scovazzo, J. Kieft, D.A. Finan, C. Koval, D. DuBois, R. Noble, Gas separations using non-hexafluorophosphate [PF6]- anion supported ionic liquid membranes, J. Memb. Sci. 238 (1–2) (2004) 57–63, https://doi.org/10.1016/j.memsci.2004.02.033.

[40] M.M. Pereira et al., Contact angles and wettability of ionic liquids on polar and non-polar surfaces, Phys. Chem. Chem. Phys. (2015), https://doi.org/10.1039/c5cp05873b.
[41] K.A. Kurnia, C.M.S.S. Neves, M.G. Freire, L.M.N.B.F. Santos, J.A.P. Coutinho, Comprehensive study on the impact of the cation alkyl side chain length on the solubility of water in ionic liquids, J. Mol. Liq. (2015), https://doi.org/10.1016/j.molliq.2015.03.040.
[42] J. Troncoso, C. A. Cerdeirin, and Y. A. Sanmamed, "Thermodynamic Properties of Imidazolium-Based Ionic Liquids : Densities , Heat Capacities , and Enthalpies of Fusion of [bmim][PF 6] and [bmim][NTf 2]," pp. 1856–1859, 2006.
[43] J. Palomar, V.R. Ferro, J.S. Torrecilla, F. Rodríguez, Density and molar volume predictions using COSMO-RS for ionic liquids. An approach to solvent design, Ind. Eng. Chem. Res. 46 (18) (2007) 6041–6048, https://doi.org/10.1021/ie070445x.
[44] Q. Liu, M. Yang, P. Yan, X. Liu, Z. Tan, and U. Welz-biermann, "Density and Surface Tension of Ionic Liquids [C n py][NTf 2] (n) 2 , 4 , 5)," pp. 4928–4930, 2010.
[45] S. Verma et al., Drastic influence of amide functionality and alkyl chain length dependent physical, thermal and structural properties of new pyridinium-amide cation based biodegradable room temperature ionic liquids, J. Mol. Struct. 1250 (2022), https://doi.org/10.1016/j.molstruc.2021.131679.
[46] A. Yadav, A. Guha, A. Pandey, M. Pal, S. Trivedi, S. Pandey, Densities and dynamic viscosities of ionic liquids having 1-butyl-3-methylimidazolium cation with different anions and bis(trifluoromethylsulfonyl)imide anion with different cations in the temperature range (283.15 to 363.15) K, J. Chem. Thermodyn. 116 (2018) 67–75, https://doi.org/10.1016/j.jct.2017.08.032.
[47] P.J. Carvalho, T. Regueira, L.M.N.B.F. Santos, J. Fernandez, J.A.P. Coutinho, Effect of water on the viscosities and densities of 1-butyl-3- methylimidazolium dicyanamide and 1-butyl-3-methylimidazolium tricyanomethane at atmospheric pressure, J. Chem. Eng. Data 55 (2) (2010) 645–652, https://doi.org/10.1021/je900632q.
[48] C.M.S.S. Neves, P.J. Carvalho, M.G. Freire, J.A.P. Coutinho, Thermophysical properties of pure and water-saturated tetradecyltrihexylphosphonium-based ionic liquids, J. Chem. Thermodyn. 43 (6) (2011) 948–957, https://doi.org/10.1016/j.jct.2011.01.016.
[49] L. J. Lozano, C. Godínez, A. P. de los Ríos, F. J. Hernández-Fernández, S. Sánchez-Segado, and F. J. Alguacil, Recent advances in supported ionic liquid membrane technology, J. Memb. Sci., vol. 376, no. 1, pp. 1–14, 2011, 10.1016/j.memsci.2011.03.036.
[50] M.G. Freire, P.J. Carvalho, R.L. Gardas, L.M.N.B.F. Santos, I.M. Marrucho, J.A.P. Coutinho, Solubility of water in tetradecyltrihexylphosphonium-based ionic liquids, J. Chem. Eng. Data 53 (10) (2008) 2378–2382, https://doi.org/10.1021/je8002805.
[51] M.G. Freire, S.P.M. Ventura, L.M.N.B.F. Santos, I.M. Marrucho, J.A.P. Coutinho, Evaluation of COSMO-RS for the prediction of LLE and VLE of water and ionic liquids binary systems, Fluid Phase Equilib. 268 (1–2) (2008) 74–84, https://doi.org/10.1016/j.fluid.2008.04.009.
[52] A. Ayad, T. Di Pietro, F. Mutelet, A. Negadi, Thermodynamic Properties of Tricyanomethanide-Based Ionic Liquids with Water: Experimental and Modelling, J. Solution Chem. 50 (4) (2021) 517–543, https://doi.org/10.1007/s10953-021-01072-9.
[53] K. Larsson, K. Binnemans, Selective extraction of metals using ionic liquids for nickel metal hydride battery recycling, Green Chem. 16 (10) (2014) 4595–4603, https://doi.org/10.1039/c3gc41930d.
[54] S. Pradhan, N. Swain, B. Sarangi, and S. Mishra, "Demonstration of extraction performance of Aliquat 336 for Europium (III) from nitrate medium," vol. 2, no. 3, pp. 256–262, 2020, [Online]. Available: https://doi.org/10.33263/Materials23.256262.
[55] "European Chemicals Agency," "ECHA," 2022. https://echa.europa.eu/.
[56] A.M. Neplenbroek, D. Bargeman, C.A. Smolders, Mechanism of supported liquid membrane degradation: emulsion formation, J. Memb. Sci. (1992), https://doi.org/10.1016/0376-7388(92)80021-B.
[57] J. Xu, R. Paimin, W. Shen, X. Wang, An investigation of solubility of Aliquat 336 in different extracted solutions, Fibers Polym. 4 (1) (2003) 27–31, https://doi.org/10.1007/BF02899326.
[58] T. Koonsang, K. Aunnankat, K. Maneeintr, U. Pancharoen, T. Wongsawa, The mutual solubility of organic-liquid membrane and aqueous phases at different water pH for the stability of SLM using Aliquat 336 as an ionic-liquid extractant, J. Mol. Liq. 292 (2019), https://doi.org/10.1016/j.molliq.2019.111363.
[59] K.F. Seip, M. Faizi, C. Vergel, A. Gjelstad, S. Pedersen-Bjergaard, Stability and efficiency of supported liquid membranes in electromembrane extraction - A link to solvent properties Microextraction Techniques, Anal. Bioanal. Chem. 406 (8) (2014) 2151–2161, https://doi.org/10.1007/s00216-013-7418-8.
[60] Q. Yang, T.S. Chung, Y. Xiao, K. Wang, The development of chemically modified P84 Co-polyimide membranes as supported liquid membrane matrix for Cu(II) removal with prolonged stability, Chem. Eng. Sci. 62 (6) (2007) 1721–1729, https://doi.org/10.1016/j.ces.2006.12.022.
[61] H. Sun, J. Yao, H. Cong, Q. Li, D. Li, B. Liu, Enhancing the stability of supported liquid membrane in phenols removal process by hydrophobic modification, Chem. Eng. Res. Des. 126 (2017) 209–216, https://doi.org/10.1016/j.cherd.2017.08.027.
[62] "National Center for Biotechnology Information," "PubChem." https://pubchem.ncbi.nlm.nih.gov/.
[63] C.M. Hansen, Hansen Solubility Parameters, A User's Handbook, 2. 2007.